NASA CONTRACTOR REPORT

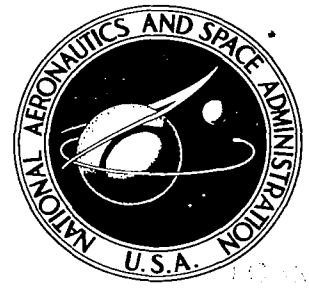

NASA CR-394

OPTIMUM EARTH RE-ENTRY CORRIDORS

by Ann Muzyka and H. Elmore Blanton

Prepared under Contract No. NAS 8-5225 *by*
RAYTHEON COMPANY
Sudbury, Mass.
for George C. Marshall Space Flight Center

NATIONAL AERONAUTICS AND SPACE ADMINISTRATION • WASHINGTON, D. C. • MARCH 1966

NASA CR-394

OPTIMUM EARTH RE-ENTRY CORRIDORS

By Ann Muzyka and H. Elmore Blanton

Prepared under Contract No. NAS 8-5225 by
RAYTHEON COMPANY
Sudbury, Mass.

for George C. Marshall Space Flight Center

NATIONAL AERONAUTICS AND SPACE ADMINISTRATION

For sale by the Clearinghouse for Federal Scientific and Technical Information
Springfield, Virginia 22151 – Price $4.00

TABLE OF CONTENTS

		Page
LIST OF FIGURES		v
LIST OF TABLES		v
FOREWORD		vii
SYNOPSIS		
1.	Introduction	1
2.	Steepest-Ascent Optimization Procedure	1
3.	Re-Entry Criteria for Manned Lifting Vehicles	2
4.	Exo -Atmospheric Altitude Ceilings on Re-Entry Trajectories	3
5.	Summary	5
PART I - EARTH RE-ENTRY CORRIDORS FOR MANNED LIFTING VEHICLE		
1.	SUMMARY	I-1
2.	INTRODUCTION	I-4
3.	LIST OF SYMBOLS	I-5
4.	PROBLEM DESCRIPTION	I-7
	4.1 Dynamic Model	I-7
	4.2 Equations of Motion	I-9
	4.3 Pilot Acceleration - Endurance Constraint	I-10
	4.4 Altitude Ceiling	I-12
	4.5 Optimization Problem	I-13
5.	PROCEDURE FOR TRAJECTORY OPTIMIZATION	I-15
6.	RESULTS	I-21
7.	CONCLUSIONS	I-28
REFERENCES		I-29
APPENDIX A - MAXIMUM AND MINIMUM RANGE TRAJECTORIES AND CONTROL HISTORIES		I-30

		Page
PART II - EXO-ATMOSPHERIC ALTITUDE CEILINGS ON OPTIMUM RE-ENTRY TRAJECTORIES		
1.	SUMMARY	II-1
2.	INTRODUCTION	II-1
3.	LIST OF SYMBOLS	II-3
4.	MATHEMATICAL MODEL	II-6
5.	OPTIMIZATION PROCEDURE	II-8
	5.1 Steepest-Ascent Procedure	II-9
	5.2 Satisfactory Skip Trajectories	II-16
	5.3 Unsatisfactory Skip Trajectories	II-17
	5.4 Escape Trajectories	II-19
6.	ANALYTIC SOLUTIONS FOR EXO - ATMOSPHERIC SEGMENTS OF PATHS	II-21
7.	CONCLUSIONS AND RECOMMENDATIONS	II-26
REFERENCES		II-28
APPENDIX A - KEPLERIAN TRAJECTORIES		II-29
APPENDIX B - COORDINATE TRANSFORMATION		II-38
APPENDIX C - ADJOINT EQUATIONS		II-47

LIST OF FIGURES

		Page
PART I		
1.	Force Diagram	I-7
2.	Lift and Drag Coefficients vs. Angle of Attack	I-8
3.	Pilot Acceleration - Endurance Limit	I-11
4.	Vehicle Range Capability	I-14
5.	Entry Arcs	I-14
6.	Bounds on Entry Flight-Path Angle vs. Entry Speed	I-22
7.	Entry Arcs for Re-Entry Speed 7833 m/sec	I-24
8.	Entry Arcs for Re-Entry Speed 11,080 m/sec	I-26
	Maximum and Minimum Range Trajectories and Control Histories (see Appendix A)	I-30
PART II		
1.	Coordinate System	II-6
2.	Types of Re-Entry Trajectories	II-8
3.	Steepest-Ascent Optimization Procedure. Flow Chart A	II-15
4.	Steepest-Ascent Optimization Procedure. Flow Chart B	II-20
5.	Re-Entry Trajectory	II-21

LIST OF TABLES

PART I		
1.	Tabulation of Results	I-21

FOREWORD

This document comprises the technical summary report covering the investigations carried out by the Raytheon Company under the provisions of Contract No. NAS 8-5225 and Modification No. 1 thereto during the period of February 11, 1963 through February 28, 1965. These investigations included the computation of optimum earth re-entry corridors for situations as defined by the customer and described in Part I of the document and the extensions of capabilities of computer programs required for these computations as reported in Part II. This work was accomplished under the technical supervision of personnel in the Aero-Astrodynamics Laboratory, Marshall Space Flight Center.

SYNOPSIS

OPTIMUM EARTH RE-ENTRY CORRIDORS

I. Introduction

The maximum capability of an aero-space vehicle can be determined quickly and accurately using the steepest-ascent optimization procedure developed at the Raytheon Company. The performance of a specific re-entry vehicle was calculated using a high-speed digital computer. This study comprises the first part of this report.

In the course of this work, the only method then available for constraining maximum altitude was found ineffective for use in escape speed re-entry problems subject to exo-atmospheric altitude ceilings. Recent extensions to the theory of the steepest-ascent technique provides a new method which can be used to give direct control over the skip-out segment of a re-entry trajectory. The second part of this report describes the application of this direct method to satisfy the constraint of an exo-atmospheric altitude upper bound on an optimal re-entry path.

2. Steepest-Ascent Optimization Procedure

The steepest-ascent optimization procedure provides the mathematical formulation for the digital computer program used here to find the re-entry capability of a given vehicle. This procedure generates a sequence of improved control histories, culminating in one which extremalizes a prescribed terminal quantity called the pay-off, while satisfying a specified set of terminal and in-flight constraints. A typical problem might be to find the maximum or minimum range for a given vehicle with prescribed limits on the total heat generated and on the magnitude of the control functions.

The mathematical model which describes the vehicle and the forces acting upon it determines the non-linear differential equations of motion. These equations can be as complicated as necessary to describe the system realistically so long as the functions are differentiable. No simplifying assumptions need be made to facilitate the solution of the system equations because they are integrated numerically. The terminal

constraints can be in the form of equations, e. g., final speed must equal Mach 2, or in the form of inequalities, e. g., final altitude must lie between 0 and 20 km. In addition to the equations of motion which provide in-flight equality constraints, there may be in-flight inequality constraints such as, aerodynamic acceleration must not exceed 10 g's anywhere on the trajectory.

The theoretical basis for the steepest-ascent procedure is the computing of influence functions for the pay-off and constraint quantities. These functions are special solutions to the differential equations adjoint to the equations of motion and they provide information on how changes in the state along the trajectory affect the terminal quantities. Such changes are then related to changes in the control histories. We then have the information needed to alter an arbitrary control history in the most efficient way, i. e. so that maximum possible increase in pay-off results for requested changes in prescribed terminal quantities and for a specified value of the square of the perturbations in the control histories. This procedure is based on linearized perturbation theory and the degree of non-linearity of the system limits the amount of valid change that can be made at one time. For this reason, it is necessary to generate a sequence of trajectories, but each is better than the previous one. The process is terminated when the amount of improvement becomes negligible.

This optimization procedure yields not only the vehicle's performance limits but, in addition, a sequence of successively improved trajectories together with their control histories. This pattern of information can be valuable in establishing appropriate guidance schemes.

3. Re-Entry Corridor for Manned Lifting Vehicle

The first task assigned in this study was to determine extreme re-entry conditions for a piloted, unpowered vehicle. This task required finding the optimal use of aerodynamic forces during the re-entry phase of an aero-space mission. The system included the constraints that the pilot not be exposed to excessive aerodynamic loads and that the vehicle remain below a pre-assigned altitude. For a set of re-entry speeds ranging from sub-orbital to escape, the extreme re-entry flight-path angles were computed as well as the extreme re-entry positions which permit arrival at a specified target. These extreme positions were located by finding the

maximum and minimum ranges of the vehicle. Thus we know, for a given re-entry velocity vector, the location of the complete set of re-entry initial positions which ensure the ability to arrive at the target.

The presence of a pilot in the vehicle precludes high aerodynamic loads. Experiments have shown that a pilot's ability to remain usefully conscious is a function of the intensities of the aerodynamic forces and their durations, the pilot's attitude with respect to the acceleration vector, and other factors. The pilot penalty function, based on an empirical relation derived from these data, provides a measure of the "acceleration dose" the pilot has taken for the entire flight. A numerical value of one represents a full dose and when incorporated as a terminal constraint serves to achieve the desired constraint on aerodynamic load.

The original steepest-ascent theory was not designed to handle directly the satisfaction of in-flight inequality constraints. The method used for controlling maximum altitude was the inclusion of an altitude penalty function in the system equations. A simple way to do this is to compute the area, in the altitude vs. time graph, which lies above the prescribed maximum altitude for each non-optimal trajectory. This area becomes a terminal quantity with desired value zero. The control program is altered to make this violation vanish by the time the optimal trajectory is found. Thus no part of the optimal trajectory is found above the altitude ceiling. This method proved satisfactory in previous studies where the altitude ceiling was well within the sensible atmosphere. The altitude ceiling specified in this problem was well outside the edge of the atmosphere, i.e., the vehicle could not be controlled using aerodynamic forces in the vicinity of the altitude upper bound. The altitude penalty function was not found to be useful for satisfying exo-atmospheric altitude ceilings in maximum range problems for vehicles entering the atmosphere with escape speeds. The skip altitude is extremely sensitive to small changes in the dynamic state of the vehicle as it leaves the atmosphere. A direct method for controlling maximum altitude was needed.

4. Exo-Atmospheric Altitude Ceilings on Re-Entry Trajectories

Recent theoretical advances at Raytheon have extended the steepest-ascent technique to include the direct handling of in-flight inequality

constraints on quantities containing the control functions, e. g., aerodynamic acceleration, as well as on functions of the state variables only, e. g. altitude. The necessary changes in the adjoint equations and discontinuities in the influence functions were derived so that optimal trajectories with segments on the constraint boundary would satisfy the necessary conditions for an extremum. The determination of optimal switching times was critical. This method was compared with the altitude penalty function method for satisfying an altitude ceiling which is well inside the sensible atmosphere. The rate of improvement for the direct method was much greater than for the penalty function method. This result is understandable because the direct method uses none of the limited amount of control perturbations while on the constraint boundary, and so concentrates all changes on the improvable part of the trajectory. Thus, the direct method is the efficient way to employ steepest-ascent.

This new method introduced the idea of an intermediate point constraint, which is treated in the same way as a terminal constraint except that its influence function is calculated only during the interval from the initial time until the associated intermediate time. The control program is altered during this interval in such a way that the pay-off quantity, the terminal constraints, and the intermediate point constraint are all improved. After the intermediate time is passed in the integration, this constraint does not influence the changes made in the remainder of the control program. For an exo-atmospheric altitude ceiling, the method of incorporating an intermediate point constraint which prescribes explicitly that the maximum altitude not exceed the altitude ceiling offers a direct means of satisfying the altitude constraint.

For a spherical earth, the direct method is even more attractive. An analytic expression exists which relates the maximum skip altitude to the dynamic state at the edge of the sensible atmosphere. Thus, an intermediate point inequality constraint can be placed on the dynamic state with which the vehicle leaves the atmosphere. Satisfaction of this condition ensures acceptable maximum altitude. The control programs are altered from the time of initial penetration of the atmosphere until the time of leaving the atmosphere subject to this intermediate point constraint. In

this way, the direct control provided by the use of an intermediate point constraint is triggered just as soon as the maximum skip altitude is known, which is at the edge of the atmosphere. An added bonus, which results from this method, is the elimination of the need of numerical integration over the Keplerian ellipse portion of the trajectory. The analytic solutions are derivable for the trajectory itself and for all the influence functions. The substitution of analytic solutions for numerical integration represents a considerable saving in computer time especially if the exo-atmospheric portion of the trajectory is large and/or the number of terminal constraints many.

5. Summary

The steepest-ascent optimization procedure is a powerful tool for determining the capability of re-entry vehicles. The first part of this study is a numerical evaluation of the performance of a given re-entry vehicle. The second part is an extension of the steepest-ascent procedure to include the direct control of maximum exo-atmospheric altitudes. The need for this extension was revealed when the use of an altitude penalty function as an indirect means of satisfying an exo-atmospheric altitude ceiling proved ineffective.

PART I

EARTH RE-ENTRY CORRIDORS FOR MANNED LIFTING VEHICLE

1. SUMMARY

A study has been made to determine the extreme re-entry flight-path angles, for various re-entry speeds, which permit safe, unpowered descent for a given manned lifting vehicle. In addition, circular arcs, called entry arcs, were located at the initial altitude of 120 km such that, for a specified initial velocity vector, entry at any point within the associated arc ensures the ability to arrive at the designated target on the surface of the earth.

The descent of the vehicle is controlled by varying the aero-dynamic forces through the angle of attack history. The presence of a pilot in the vehicle precludes excessive aerodynamic loads. A pilot tolerance function, which is a measure of a pilot's ability to remain usefully conscious and is a function of both the intensity and duration of the aerodynamic acceleration is included as a constraint in the system equations. This condition determined the steepness of the entry flight-path angle.

The re-entry speeds range from sub-orbital to escape speeds. A vehicle entering the atmosphere at parabolic speed and shallow flight-path angle may skip out of the atmosphere. In order to exclude trajectories with extremely high skip altitudes, an altitude ceiling of 150 km. was imposed upon the trajectory. This condition served to limit the shallowness of the entry flight-path angle.

The endpoints of the entry arcs, which determine the locus of all possible initial points of trajectories satisfying the constraints and terminating on the target, were found by computing the range capability of the vehicle. By placing the terminal points of the maximum and minimum range trajectories at the target, the initial points of these trajectories then locate the endpoints of the entry arcs. There is an arc associated with each re-entry velocity vector. Thus, if the given vehicle, having the specified entry velocity, penetrates the atmosphere outside this arc, the pilot will not be able to reach the target satisfying the pilot and altitude constraints, The extreme trajectories were determined using the steepest-ascent optimization technique with IBM 7090 and 7094 high speed computers. This method generates a sequence of improved control programs culminating in the required extremal trajectory.

The vehicle is considered a mass particle of weight 8500 lbs, which moves with respect to a spherical, non-rotating earth under the action of the inverse square gravitational field, its lift and its drag. The lift and drag coefficients are functions of the angle of attack and maximum lift to drag ratio is 0.82. The reference area is 12.97 square meters. ARDC Model Atmosphere 1956 provided the variation of air density with altitude. The entry point is 120 km. above the surface of the earth and no point of the optimal trajectories has altitude exceeding 150 km. nor is the pilot subjected to an excessive "acceleration dose."

The results of the study show that for entry speeds as low as 750 m./sec., there are no restrictions on entry flight-path angle and the vehicle must enter the atmosphere within one degree of the target if the re-entry velocity is horizontal. Thus, the maximum maneuverability is negligible. When the entry speed is increased to 3500 m./sec., consideration for the pilot limits the entry flight-path angle to 110° measured from the local vertical. For this steepest entry angle, the vehicle must penetrate the atmosphere between 2.3° and 3.1° from the target. For horizontal entry, the entry arc ranges from 4.8° to 7.3° measured from the target. When the entry speed is circular, here taken as 7833 m./sec., the vehicle can be kept within the atmosphere for any entry angle larger than 90°. For a typical shallow entry of 90.5°, the vehicle requires at least 46° of range for its descent and cannot be kept in the air for more than 138°. The steepest allowable entry angle is 101.75° and then the entry arc shrinks to 8° with the closer endpoint a mere 8° from the target.

The system becomes very sensitive when the re-entry takes place at parabolic speeds, i.e. 11080 m./sec. To satisfy the pilot and altitude constraints, the entry flight-path angle must fall within the narrow range of 94.71° to 99.8° and for these entry angles, the closer endpoint of the entry arcs are 22° and 15° away from the target respectively. The farther endpoint, determined by the maximum range trajectories, were difficult to locate. They are at least as far as 160° and 110° away from the target for the shallowest and steepest entries respectively. The altitude constraint of 150 km. proved difficult to satisfy. The criterion to maximize range alters the control program

in the direction to produce skip-out. An altitude penalty function was used to control this tendancy but slight changes in the consecutive control programs resulted in alternate satisfaction and violation of the exo-atmospheric altitude ceiling. Another approach was needed. Part II of this study discusses the proposed solution to this problem: the intermediate point constraint method of controlling exo-atmospheric skips by constraining that specific function of the dynamic state of the vehicle at the edge of the atmosphere, which determines maximum skip altitude.

2. INTRODUCTION

This study is part of the general abort re-entry problem. The trajectory of a space vehicle begins with a boost phase which transports the vehicle through the atmosphere and into space where it enters a powered and/or cruise phase through space. Somewhere along the trajectory, a decision to abort may be necessary. The point of no return, i.e., the last time a successful abort may be initiated, depends on the ability of the vehicle to turn around and re-enter the atmosphere with a velocity which ensures a safe descent to a specified landing site on the surface of the earth. The constraints on the unpowered atmospheric portion of the return trajectory determine the bounds on the speed and flight-path angle at the entry point as well as its location with respect to the landing point. These bounds on the initial conditions of the atmospheric phase of the trajectory become bounds on the terminal conditions of the exo-atmospheric part of the return trajectory. These restrictions together with the engine capability of the vehicle determine the limits on the dynamic state for the initiation of a successful abort. The bounds, which define the vehicle's capability, must be found before a manned space mission can be planned.

This report is concerned with finding the bounds on the dynamic state at the edge of the atmosphere which ensure a safe unpowered descent to a specified target near the surface of the earth. These bounds depend on the amount of control available to the pilot through the lift and drag characteristics of the vehicle. They are also influenced by the limits on aerodynamic load imposed upon the system for the safety of the pilot and on the exo-atmospheric altitude ceiling which serves to exclude trajectories with excessive skip altitudes. The initial altitude is specified near the boundary of the sensible atmosphere. Under these conditions, the bounds on the initial flight-path angle for specified initial speeds was sought. At high entry speeds, the steepness of the entry angle is limited by consideration for the pilot and the shallowness by the skip out ceiling. In addition, the locus of regions at the edge of the atmosphere was sought for each extreme entry velocity vector such that entry of the atmosphere at a point within the region with the specified velocity guarantees the ability to arrive at the target. These regions serve as terminal target areas for the preceding exo-atmospheric portion of the flight and are thus interfaces for the complete aerospace problem. The information obtained here for finding entry regions with respect to a specified target can be used for the converse problem of locating targets or landing sites for a specified entry position.

3. LIST OF SYMBOLS

A	altitude penalty function
C_D	drag coefficient
C_L	lift coefficient
D	drag
G	vector of the partial derivatives of state variable rates with respect to control function
L	lift
P	pilot penalty function
R	earth radius
S	reference area
T	final time
V	vehicle speed
V_o	initial (re-entry) vehicle speed
a	aerodynamic acceleration
g	gravitational acceleration
g_o	g at surface of the earth
h	altitude
h_1	reference altitude
m	vehicle mass
t	time
u	step function
α	control variable, angle of attack
$\delta\alpha$	change in control variable
θ	flight-path angle
θ_o	initial (re-entry) flight-path angle
λ	influence function

LIST OF SYMBOLS (Continued)

ρ	density of air
τ	pilot acceleration-endurance time
ϕ	angular displacement, range
ψ	terminal constraint

4. PROBLEM DESCRIPTION

4.1 Dynamic Model

The vehicle is considered to be a particle of constant mass which moves in a plane with respect to a spherical, non-rotating earth. It is subject to the action of three forces: the inverse-square gravitational field of the earth, its lift, and its drag. The descent of the vehicle is controlled by varying the lift and drag forces. The variation of air density with respect to altitude is included. The force diagram is shown in Figure 1.

FORCE DIAGRAM

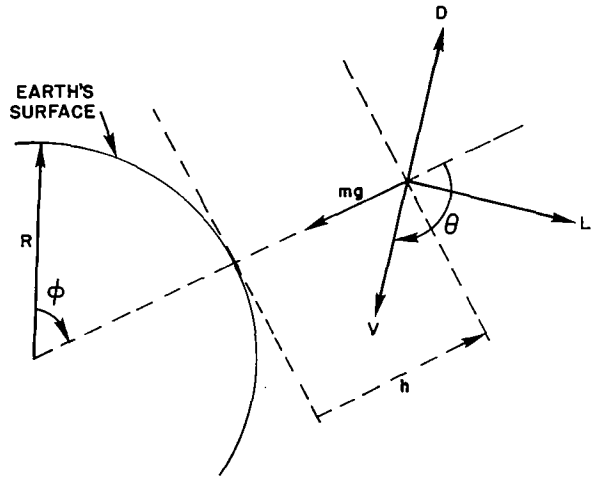

FIGURE 1

The weight of the vehicle is 8500 pounds and its reference area is 12.97 square meters. The aerodynamic coefficients are functions of the control variable, α , as shown in Figure 2. The maximum lift-to-drag ratio is 0.82 which occurs at a = 50°. During this study, the angle of attack was constrained to the interval of -70° to 70° because this interval includes the extreme variations in lift, drag, and lift-to-drag ratio.

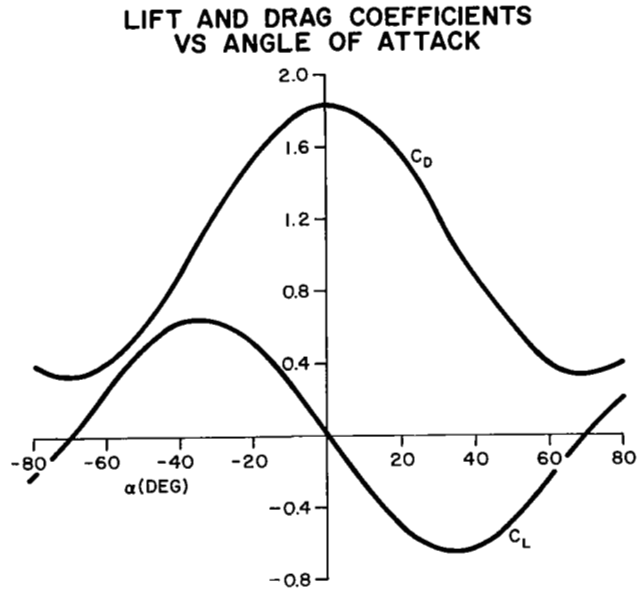

FIGURE 2

Below Mach 2, the aerodynamic coefficients are functions not only of angle of attack but also of Mach number. In view of this consideration, a speed of Mach 2 served as the stopping condition for the computing. This speed occurs at altitudes compatible with the initiation of the landing phase.

4.2 Equations of Motion

$$m\dot{V} = -D - mg\cos\theta$$

$$mV(\dot{\theta} + \dot{\phi}) = -L + mg\sin\theta$$

$$(R + h)\dot{\phi} = V\sin\theta$$

$$\dot{h} = V\cos\theta$$

where

$$g = g_o\left(\frac{R}{R + h}\right)^2$$

$$D = \frac{1}{2} C_D(\alpha)\,\rho(h)\,V^2 S$$

$$L = \frac{1}{2} C_L(\alpha)\,\rho(h)\,V^2 S$$

and

$\rho(h)$ is given by ARDC Model Atmosphere 1956.

$C_D(\alpha)$ and $C_L(\alpha)$ are shown in Figure 2.

$g_o = 9.815$ m./sec.^{2}

$R = 6.371 \times 10^6$ m.

$S = 12.97$ m.^{2}

$m = 393$ kg. sec^2/m.

4.3 Pilot Acceleration-Endurance Constraint

For a manned re-entry, control programs which produce excessive aerodynamic accelerations must be excluded. This condition is imposed during the solution procedure in the following way. A man's ability to remain usefully conscious is a function of both the aerodynamic accelerations he experiences and their durations. It has been shown that he can tolerate quite high accelerations if they are sufficiently brief. The dimensionless aerodynamic acceleration, a, is defined by

$$a = \frac{\sqrt{L^2 + D^2}}{mg_o}$$

Experimental data may be used to derive the endurance limit $\tau(a)$ of experienced test pilots to given aerodynamic accelerations. The pilot acceleration-endurance function, $\tau(a)$, used in this study is shown in Figure 3. This function was derived principally from information in References 1-3. The more recent data in References 4 and 5 reveal that the function of Figure 3 is conservative by factors from 2 to 5, in terms of permissible time for a given acceleration, if the pilot is oriented in the most favorable attitude. In the current study, however, the attitude of the vehicle is subject to wide variations in some maneuvers. If the pilot is exposed to similar variations in attitude, he may experience situations where, according to Reference 5, his endurance is significantly less than that shown in Figure 3. It is believed, however, that the $\tau(a)$ relation employed in the current study represents a reasonable compromise for the specification of pilot endurance to acceleration. As a refinement in the future, acceleration endurance might be introduced as a function of both aerodynamic acceleration and pilot attitude.

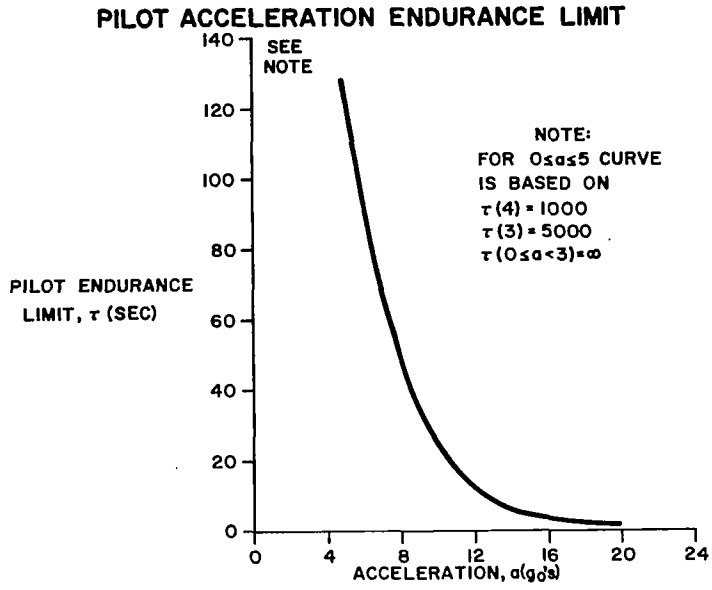

FIGURE 3

By adding the equation:

$$\dot{P} = \frac{1}{\tau\,(a)}$$

to the equations of motion, the "acceleration dose" or terminal value of the "pilot penalty function" is given by

$$P = \int_0^T \frac{1}{\tau\,(a)}\,dt,$$

where T is the time of flight. When this quantity becomes 1, the pilot is assumed to have had a full dose of acceleration; therefore, he should not be exposed to further accelerations which would increase this dose, if he is to function usefully. Thus, a terminal constraint is $\dot{P} \leq 1$.

4.4 Altitude Ceiling

One of the constraints on the problem is that no point of the optimal trajectory shall have altitude exceeding 150 km. For this vehicle and the range of entry speeds considered, this altitude is considerably beyond the "edge" of the sensible atmosphere. The aerodynamic control is negligible in this region. The vehicle cannot control its motion during its skip phase. The control program must be adjusted before the vehicle leaves the atmosphere so that its maximum skip altitude does not exceed 150 km.

A standard way of satisfying this condition is to add to the equations of motion, an altitude penalty function. There are many ways to define such a function. A useful one is:

$$\dot{A} = \left(\frac{h - h_1}{h_1} \right)^2 u \quad (h - h_1)$$

where the u is a step function defined as:

$$u(r) = 0 \quad \text{for} \quad r < 0$$
$$u(r) = 1 \quad \text{for} \quad r \geq 0$$

Thus the quantity:

$$A = \int_0^T \left(\frac{h - h_1}{h_1} \right)^2 u \quad (h - h_1) \, dt$$

is a measure of the portion of the trajectory above a reference altitude h_1. If the squared term were raised to the first power and h_1 set equal to 150 km, A would be proportional to the area, in the altitude versus time graph, which lies above the maximum prescribed altitude and thus could be considered the amount of altitude ceiling violation over the entire trajectory. The excess altitude is squared in order to penalize gross altitude ceiling violations more heavily than small ones and h_1 may sometimes be set to a number smaller than the altitude ceiling. The altitude constraint is satisfied when A is zero. Thus A can be used as a terminal constraint in the steepest-ascent procedure.

4.5 Optimization Problem

The problem to be solved was two-fold. The first was to find the limits on the re-entry flight—path angle for each of four re-entry speeds. These limits are imposed upon the entry angle by the requirement that the terminal value of the pilot penalty function not exceed 1 and the terminal value of the altitude penalty function be zero. The steepness of the entry angle was determined by the pilot constraint. The entry angle was increased in discrete steps and for each, a pilot penalty minimization problem solved. The upper bound was established as the largest entry angle for which a successful minimization yielded an "acceleration dose" less than or equal to 1. The lower bound, or shallowest entry angle was determined by the altitude ceiling. It was found by using the control which produced maximum negative lift. The minimum entry angle is the smallest one which satisfies the altitude ceiling when the control is set for maximum negative lift.

The second problem was to find the locus of all points at the initial altitude such that arrival of the vehicle at one of these points with the specified velocity vector ensures the ability to reach a given target. Thus, arrival of the vehicle outisde this "entry arc" with the specified velocity will result in overshooting or undershooting the target. The minimum range needed by the vehicle to traverse the atmosphere determines the overshoot boundary, while its maximum range sets the undershoot boundary. The endpoints of the entry arcs are thus located by finding the range capability of the vehicle for the shallowest and steepest entry angle for each entry speed. Since there are four entry speeds : 750 m./sec., 3500 m./sec., 7833 m./sec. and 11,080 m./sec. this requires finding eight entry arcs and thus a total of 16 optimization problems were solved.

The method used to locate entry arcs is shown in Figures 4 and 5. For a given re-entry velocity vector, i.e. specified initial speed and initial flight-path angle, the maximum and minimum ranges are computed subject to a limit of 1 on the "acceleration dose" given the pilot and an altitude ceiling of 150 km. The initial altitude is 120 km. and the stopping condition or final time is determined when the speed reaches Mach 2. Figure 4 shows typical maximum and minimum range trajectories, starting from the same initial point. The same trajectories are shown in Figure 5, displaced so that they go through the same terminal point. Thus, their initial points become the end points of the entry arc. If the initial altitude of the vehicle is anywhere on the arc $E_1 E_2$ and the vehicle has the specified initial velocity,

then arrival at the target can be achieved. If the initial altitude is outside the entry arc, then the vehicle will undershoot or overshoot the target.

Vehicle Range Capability

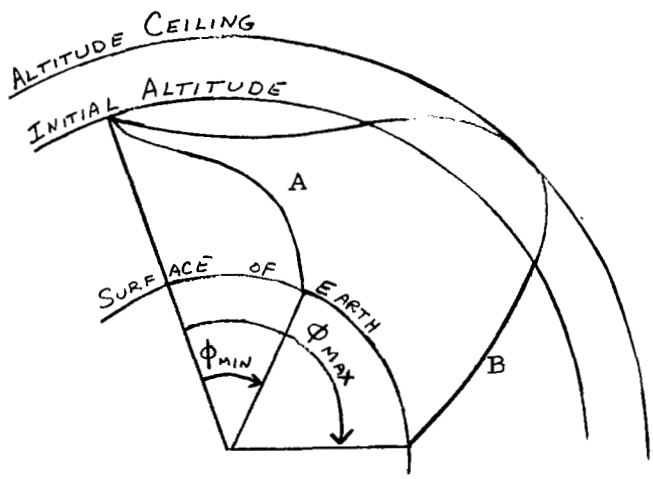

A = Minimum Range Trajectory

B = Maximum Range Trajectory

Initial Velocity Vector Specified

Figure 4.

Entry Arcs

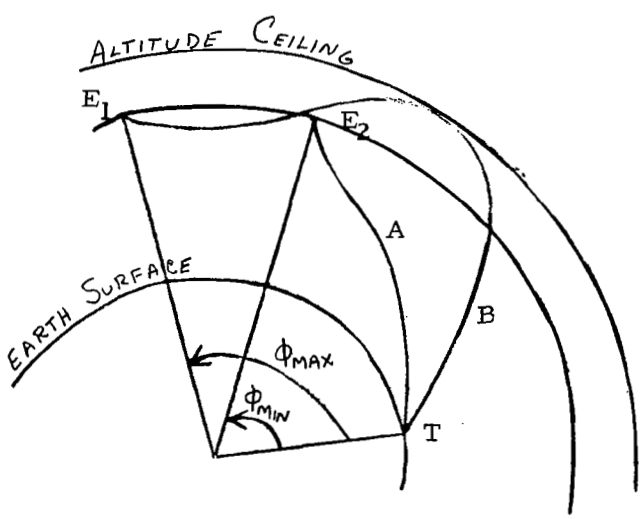

A = Minimum Range Trajectory

B = Maximum Range Trajectory

T = Target Location

Arc $E_1 E_2$ is Entry Arc for Specified Initial Velocity Vector.

Figure 5.

5. PROCEDURE FOR TRAJECTORY OPTIMIZATION

The differential equations of motion together with the pilot and altitude penalty functions form the non-linear system equations which describe the problem. They are:

$$\dot{V} = -\frac{1}{2m} C_D(\alpha)\, \rho(h)\, V^2 S - g_o \left(\frac{R}{R+h}\right)^2 \cos\theta$$

$$\dot{\theta} = -\frac{1}{2m} C_L(\alpha)\, \rho(h)\, V S + \frac{g_o}{V} \left(\frac{R}{R+h}\right)^2 \sin\theta - \frac{V \sin\theta}{R+h}$$

$$\dot{\phi} = \frac{V \sin\theta}{R+h}$$

$$\dot{h} = V \cos\theta$$

$$\dot{P} = \frac{1}{\tau(\alpha)}$$

$$\dot{A} = \left(\frac{h - h_1}{h_1}\right)^2 u(h - h_1)$$

This system of differential equations could be solved numerically if the initial conditions were specified and if the control program $\alpha(t)$ were known. The steepest-ascent optimization procedure generates a sequence of successively improved control histories which culminate in the optimal control program. An optimal control program is one which extremalizes a specified terminal quantity.

The process starts with an arbitrary control function $\alpha_o(t)$. It is arbitrary in the mathematical sense but in practice requires that engineering experience with the given mission provide a nominal control program which keeps the resulting trajectory in the right region. From specified initial

conditions, the system equations are integrated numerically using the nominal control program until the terminal condition which determines final time is reached. We then have a re-entry trajectory. Let us assume range is to be maximized subject to the terminal conditions the $P \leq 1$ and $A = 0$, i.e. the pilot is not to receive more than one full dose of acceleration and the altitude ceiling is to be satisfied. Our first re-entry trajectory will not, in general, maximize the range nor satisfy the limits on P and A. For this reason, the control program $\alpha_o(t)$ must now be improved. The criterion for improvement is that the next trajectory show maximum increase in range for requested improvements in P and A, hence the name steepest-ascent. The theory for computing $\delta\alpha(t)$ which when added to $\alpha_o(t)$ to produce a new control program $\alpha_1(t)$ that does just this is based on small perturbations about the nominal trajectory. There is then a limit on the amount of change, measured by the expression

$$\int_{t_o}^{T} \left[\delta\alpha(t) \right]^2 dt$$

which can be made and therefore on the requested improvements in the terminal conditions and the expected increase in the range. Thus, the process must be repeated, each iteration improving the control program until no further improvement can be made. The final control program yields maximum range and satisfies the pilot and altitude constraints.

The derivation of the expression for $\delta\alpha(t)$ is given in Ref. 6. The scheme for computing $\delta\alpha(t)$ will be summarized here and the mathematical justification for it is given in Part II of this report.

The system equations are integrated from t_o using a given set of initial conditions and the nominal control program $\alpha_o(t)$ until the final time T. A terminal constraint is chosen to be the stopping condition. In this problem it is V = Mach 2. This condition is always satisfied. The conditions which are not, in general, satisfied are $\phi(T)$ = maximum, $P \leq 1$ and $A = 0$.

We can get information on how $d\phi(T)$, dP and dA are related to $\delta\alpha(t)$ by finding special solutions to the adjoint differential equations of the given system. These are:

$$\dot{\lambda}_V = \frac{1}{m} C_D \rho V S \lambda_V + \left[\frac{1}{2m} C_L \rho S + \frac{g_o}{V^2} \left(\frac{R}{R+h} \right)^2 \sin\theta \right.$$

$$\left. + \frac{\sin\theta}{R+h} \right] \lambda_\theta - \frac{\sin\theta}{R+h} \lambda_\phi - (\cos\theta)\, \lambda_h$$

$$- \frac{2a}{V} \frac{d}{da} \left(\frac{1}{\tau} \right) \lambda_P$$

$$\dot{\lambda}_\theta = - g_o \left(\frac{R}{R+h} \right)^2 (\sin\theta)\, \lambda_V - \left[\frac{g_o}{V} \left(\frac{R}{R+h} \right)^2 \cos\theta - \frac{V\cos\theta}{R+h} \right] \lambda_\theta$$

$$- \frac{V\cos\theta}{R+h} \lambda_\phi + (V \sin\theta)\, \lambda_h$$

$$\dot{\lambda}_\phi = 0 \text{ so } \lambda_\phi = \text{constant}$$

$$\dot{\lambda}_h = \left[\frac{1}{2m} C_D \frac{d\rho}{dh} V^2 S - \frac{2 g_o}{R} \left(\frac{R}{R+h} \right)^3 \cos\theta \right] \lambda_V$$

$$+ \left[\frac{1}{2m} C_L \frac{d\rho}{dh} V S + \frac{2 g_o}{V R} \left(\frac{R}{R+h} \right)^3 \sin\theta - \frac{V \sin\theta}{(R+h)^2} \right] \lambda_\theta$$

$$+ \frac{V \sin\theta}{(R+h)^2} \lambda_\phi - \frac{a}{\rho} \frac{d\rho}{dh} \frac{d}{da} \left(\frac{1}{\tau} \right) \lambda_P$$

$$- \frac{2}{h_1^2} (h - h_1)\, u\, (h - h_1)\, \lambda_A$$

$$\dot{\lambda}_P = 0 \text{ so } \lambda_P = \text{constant}$$

$$\dot{\lambda}_A = 0 \text{ so } \lambda_A = \text{constant}$$

This linear set of differential equations is integrated backward from T to t_o, three times giving the three influence functions, $\underline{\lambda}^{\phi}(t)$, $\underline{\lambda}^{P}(t)$, $\underline{\lambda}^{A}(t)$ where each vector has the six components: $\lambda_V(t)$, $\lambda_\theta(t)$, $\lambda_\phi(t)$, $\lambda_R(t)$, $\lambda_P(t)$ and $\lambda_A(t)$. The "initial" conditions for these functions are:

$$\underline{\lambda}^{\phi}(T) = \begin{bmatrix} \left(-\frac{\dot{\phi}}{\dot{V}}\right) \\ 0 \\ 1 \\ 0 \\ 0 \\ 0 \end{bmatrix}, \quad \underline{\lambda}^{P}(T) = \begin{bmatrix} \left(-\frac{\dot{P}}{\dot{V}}\right) \\ 0 \\ 0 \\ 0 \\ 1 \\ 0 \end{bmatrix}, \quad \underline{\lambda}^{A}(T) = \begin{bmatrix} \left(-\frac{\dot{A}}{\dot{V}}\right) \\ 0 \\ 0 \\ 0 \\ 0 \\ 1 \end{bmatrix}$$

where $\dot{\phi}$, $\dot{V}$, $\dot{P}$, $\dot{A}$ are evaluated at T. The two influence functions for the terminal constraints $\underline{\lambda}^{P}(t)$ and $\underline{\lambda}^{A}(t)$ are combined to give the 6×2 matrix $\lambda^{\psi}(t)$.

The adjoint equations were formed using partial derivatives of all the state variable rates with respect to all the state variables. We also need partial derivatives of all the state variables with respect to the control variable. This is given by the vector $G(t)$ which is

$$G(t) = \begin{bmatrix} -\frac{1}{2m}\frac{dC_D}{d\alpha}\rho V^2 S \\ -\frac{1}{2m}\frac{dC_L}{d\alpha}\rho V S \\ 0 \\ 0 \\ \frac{a}{2}\frac{d}{d\alpha}\left(\frac{1}{\tau}\right)\frac{d}{d\alpha}\ln\left(C_D^2 + C_L^2\right) \\ 0 \end{bmatrix}$$

We now have the information we need to compute the change in the control program. It is:

$$\delta a(t) = G' \left(\underline{\lambda}^{\phi}(t) - \lambda^{\psi}(t)\, I_{\psi\psi}^{-1}\, I_{\psi\phi} \right) \sqrt{\frac{(dp)^2 - d\psi'\, I_{\psi\psi}^{-1}\, d\psi}{I_{\phi\phi} - I_{\phi\phi}'\, I_{\psi\psi}^{-1}\, I_{\psi\phi}}}$$

$$+ G' \lambda^{\psi}(t)\, I_{\psi\psi}^{-1}\, d\psi$$

where $I_{\psi\psi} \equiv \int_{t_o}^{T} (\lambda^{\psi})'\, G\, G'\, \lambda^{\psi}\, dt$

$$I_{\psi\phi} \equiv \int_{t_o}^{T} (\lambda^{\psi})'\, G\, G'\, \underline{\lambda}^{\phi}\, dt$$

$$I_{\phi\phi} \equiv \int_{t_o}^{T} (\underline{\lambda}^{\phi})'\, G\, G'\, \underline{\lambda}^{\phi}\, dt$$

$$(dp)^2 \equiv \int_{t_o}^{T} \left[\delta a(t) \right]^2 dt$$

$$d\psi \equiv \begin{bmatrix} dP \\ dA \end{bmatrix}$$

dP and dA are the requested changes in the pilot and altitude constraints and $(dp)^2$ is the requested amount of change in the control program. If $(dp)^2$ is chosen not so large that the linearity assumptions are violated, then the next re-entry trajectory produced by $a_1(t) = a_o(t) + \delta a(t)$ will have the

largest possible increase in range for this amount of control change and the pilot and altitude penalty functions will have values $P + dP$ and $A + dA$ respectively. The entire procedure is repeated using $\alpha_1(t)$ in place of $\alpha_o(t)$. In this way, a sequence of control programs are generated, each better than the previous one. The procedure is terminated when the amount of improvement becomes negligible.

6. RESULTS

The results are tabulated in Table 1. For a given entry velocity, the angular distance between the target and the re-entry point nearest to the target is indicated in the Minimum Range column. If the vehicle enters the atmosphere at this distance from the target, the descent must be made using the α program associated with the minimum-range trajectory. An entry closer to the target will cause overshoot because the steepness of the trajectory is limited by the pilot penalty function. Similarly, the numbers in the Maximum Range column indicate the farthest from the target that entry may occur. The entry arc is the circular arc at the specified initial altitude of 120 km. joining the nearest and farthest possible re-entry points. Entry at any point within this arc with the associated initial speed and flight-path angle ensures the ability to arrive at the target. The entry flight-path angle, which is the direction of the initial velocity vector measured counterclockwise from the local vertical, can be confined to lie between 90° and 180°. The trajectory for an entry flight-path angle lying between 180° and 270° is the same as for its mirror image in the 90° to 180° range.

Table 1. Tabulation of Results

Entry Speed (m./sec.)	Entry Flight-Path Angle (degrees)	Minimum Range (degrees)	Maximum Range (degrees)	Entry-Arc Length (degrees)
750	90 180	0.93 0	1.05 ±0.05	0.12 0.10
3500	90 110	4.8 2.3	7.3 3.1	2.5 0.8
7833	90.50 101.75	46 8	138 16	92 8
11080	94.71 99.8	22 15	160* 110*	138 95

* See discussion in text.

The re-entry corridor, as it appears in the initial-flight-path-angle, initial-speed plane, is shown graphically in Figure 6.

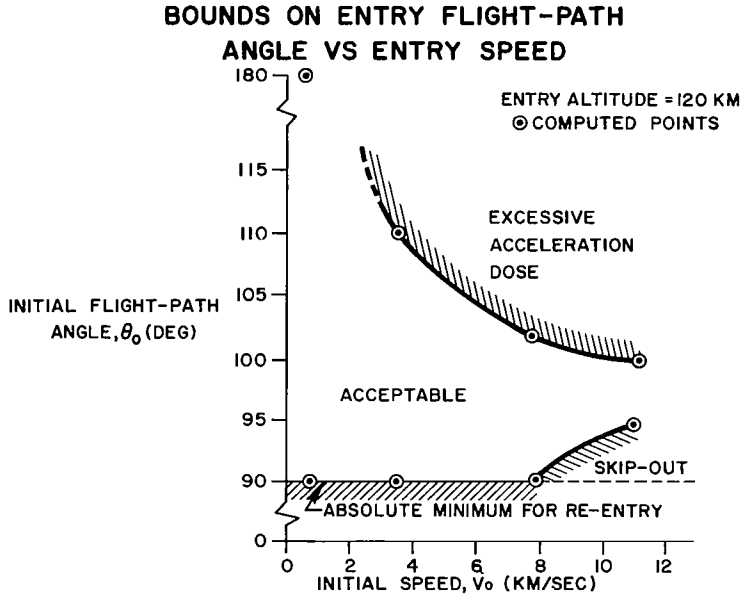

FIGURE 6

For the lowest entry speed studied, 750 m./sec., there is no restriction on the initial flight-path angle. The vehicle can enter the atmosphere with a horizontal velocity or one which is straight down, but the range and entry-arc length are so small as to be negligible when compared with the performance at higher speeds.

The steepest entry angle for an entry speed of 3500 m./sec. is approximately 110°. At this entry angle, the pilot penalty constraint can be held to 1 for maximum and minimum ranges through appropriate modulation of the α program. A critical search was not made to verify the possibility of steeper entries because available information concerning the entire abort-trajectory problem indicated that re-entries for initial speeds of roughly 3500 m./sec. most likely will occur for angles less than 110°. The range and entry-arc capabilities at this speed may be of some significance for an entry at an angle of 90° but they both decrease drastically as the entry angle becomes steeper.

For true circular entry speed, the shallowest possible entry angle is undefined. A horizontal circular velocity, $\theta_o = 90^{\circ}$, results in a circular orbit and consequently no entry if the effects of aerodynamic drag are absent. Any initial flight-path angle greater than 90° will result in re-entry, and the closer this angle is to 90°, the larger the maximum range. Similarly, a slight reduction in initial speed and/or the presence of slight aerodynamic drag at the specified initial altitude will lead to entry. For the solutions obtained during this study, the initial speed was circular for the entry altitude, but the atmospheric density, and hence drag, were defined to above this altitude in accordance with the ARDC Model Atmosphere, 1956.

In the circular-speed-entry studies, an arbitrarily selected shallow initial angle of 90.50° was found to lead to a maximum range of only 138°. As the entry angle becomes steeper, the maximum range decreases until it is only 16° for steepest permissible entry, $\theta_o = 101.75^{\circ}$. The minimum ranges and the entry-arc lengths also are markedly less for the steeper

entry angles. This situation is illustrated in Figure 7. It is significant to note that the entry arcs for the extreme entry angles do not overlap; consequently, several target areas will be necessary to effect successful recovery of space vehicles re-entering at circular speed if initial flight-path angles lie anywhere between the limits of 90° and 101.75°.

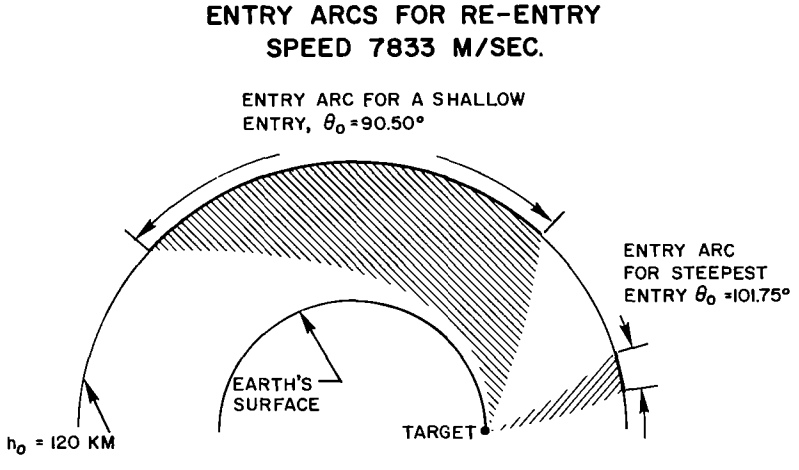

FIGURE 7

When a vehicle travelling at supercircular speed re-enters the atmosphere at a shallow flight-path angle, the aerodynamically produced deceleration may be insufficient to prevent the vehicle from rising above a specified altitude limit. Thus, the re-entry problem reduces to the determination of the shallowest initial angle that leads to the satisfaction of the altitude restriction when the vehicle is flown with maximum negative lift. Through the use of results of theoretical analyses, as verified by numerical solutions, it was established that, for an entry speed of 11,080 m./sec. (essentially escape speed), acceptable re-entry can be accomplished for an entry angle as shallow as 94.71°, but not for one of 94.55°, when the altitude limit is 150 km. In lieu of attempting to define θ_o more exactly within this narrow range, 94.71° was taken as the shallowest initial flight-path angle at this speed.

The steepest entry angle at escape speed is limited by the pilot acceleration dose during the initial dive into the atmosphere. This dose is critically dependent on the precise modulation of the angle-of-attack program. For an entry angle of 99.8° an acceptable pilot-penalty value was achieved for both minimum and maximum range trajectories. Among the many trajectories evolved during the study of performance for steeper initial flight-path angles, none yielded an acceleration dose as low as 1.

Minimum-range capability for escape-velocity entries also is limited by the pilot acceleration dose. For the entry angles studied, this range decreased from 22° for 94.71° to 15° for 99.8°. In the case of the shallow entry angle of 94.71°, a sufficient margin of negative lift was available to prevent the minimum-range trajectory from leaving the atmosphere following initial entry. Of course, for the actual shallowest permissible entry angle, which is between 94.55° and 94.71°, the minimum-range trajectory would include a rise to the specified maximum altitude of 150 km and the resulting range would be substantially greater than 22°.

The computation of the maximum range for entries at escape speed becomes particularly difficult as the steepness of the entry angle increases. In these situations, the angle-of-attack program during the first 10% or less of the total flight time must be modulated extremely accurately in such a way that both the pilot-penalty and maximum-altitude restrictions are satisfied in a manner compatible with maximization of the range. The total pilot penalty is realized during roughly 2% of the flight time shortly after initial entry into the atmosphere, and the maximum altitude restriction, 150 km, occurs later in the flight during a long interval when the aerodynamic forces are negligible, thus complicating the solution process. During this study, the range capability was computed both by optimizing the performance during the entire time of flight and by combining extremal solutions for appropriately defined portions of the over-all trajectory. Cross checks were made to establish the compatibility of these approaches and to ensure the relative validity of the answers. The maximum ranges given in Table 1 represent the "best" answers obtained. These ranges definitely are realizable under the specified conditions and perhaps can be increased through appropriate changes in the angle-of-attack program early in the flight.

The entry arcs for escape-speed entry are shown in Figure 8. For entry angles of 94.71° and 99.8°, the entry arcs overlap to a large extent indicating the feasibility of using a single recovery area.

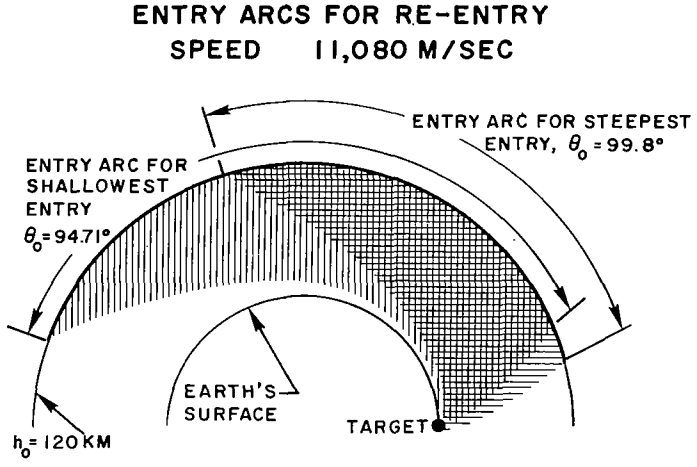

FIGURE 8

In aborts during space missions, of course, the re-entry velocities are not subject to close control; they will lie between broad limits which are determined by many factors. Based on the results given in Table 1, if the speeds may be anywhere in range from zero up to escape and entry flight-path angles are unrestricted, recovery facilities would have to be provided on a continuous basis throughout possible re-entry areas. As the range of expected speeds decreases, and as probable flight-path angles are defined, projections may be made as to the discrete number of landing sites needed to effect successful recovery.

7. CONCLUSIONS

As re-entry speeds increase from 750 m./sec. to escape speeds, restrictions arise on the possible re-entry flight-path angles. The shallowness of the entry, for supercircular entry speeds, is limited by the tendency of the vehicle to skip out; the steepness of the entry for all except the lowest speeds, by the "acceleration-dose" constraint. Stringent restrictions on initial flight-path angles which occur for escape-speed entries are coupled with wide tolerances on re-entry position. Re-entry speeds and flight-path angles must be limited more than indicated by the results reported here if a small number of landing sites is to offer a high probability of successfully recovering aborted spacecraft.

The results of this study define extreme re-entry conditions for the specified vehicle when subject only to pilot-acceleration-dose and altitude constraints. The re-entry corridor may be changed if any of the following considerations are included: the total heat and/or heating rate is constrained; the pilot-acceleration-endurance function includes pilot attitude dependence; or the magnitude of the angle of attack is limited.

Although the penalty function method has been used successfully to satisfy altitude ceilings which lie within the atmosphere, it was not effective in controlling skips out of the atmosphere. A more direct method yielding firmer control of the maximum altitude appeared to be necessary. Since the vehicle is unpowered, its entire exo-atmospheric trajectory is determined by the dynamic state with which it leaves the atmosphere. Thus the constraint should not be on a terminal quantity as it is using a penalty function but directly on this dynamic state. Part II of this report describes a new method which relates the maximum skip altitude to the dynamic state at the edge of the atmosphere and constraints this critical state. In this way, the steepest-ascent optimization procedure is used in a much more efficient manner and the solution of escape speed re-entry problems is facilitated.

REFERENCES

1. Bryson, A. E., and Denham, W. F., "Guidance Scheme for Supercircular Re-Entry of a Lifting Vehicle," American Rocket Society Journal, Vol. 32, No. 6, June 1962, pp 894-898.

2. Konecci, E. B., "Manned Space Cabin Systems," Chapter 4 of Advances in Space Sciences, Vol. 1, R. I. Ordway III, ed., Academic Press, N. Y., 1959.

3. Hegenwald, J., and Oishi, S., Human Tolerance to Acceleration, North American Aviation, Inc., 1957.

4. Creer, B. Y., Smedal, H. A., and Wingrove, R. C., Centrifuge Study of Pilot Tolerance to Acceleration and the Effects of Acceleration on Pilot Performance, National Aeronautics and Space Administration, Technical Note NASA TN-D-337, 1960.

5. Chambers, R. M., and Hitchcock, L., Jr., "Effects of High G Conditions on Pilot Performance," Proceedings of the National Meeting on Manned Space Flight, co-sponsored by National Aeronautics and Space Administration and Institute of the Aerospace Sciences, St. Louis, April 30 - May 2, 1963, pp 204-217.

6. Bryson, A. E., and Denham, W. F., "A Steepest-Ascent Method for Solving Optimum Programming Problems," Trans. of ASME, Series E: Journal of Applied Mechanics, Vol. 29, No. 2, June 1962, pp 247-257; also Raytheon Company, Report BR-1303, Aug. 10, 1961.

7. Chapman, D. R., An Approximate Analytical Method for Studying Entry into Planetary Atmospheres, National Aeronautics and Space Administration, Technical Report NASA TR R-11, 1959.

8. Chapman, D. R., An Analysis of the Corridor and Guidance Requirements for Supercircular Entry into Planetary Atmospheres, National Aeronautics and Space Administration, Technical Report NASA TR R-55, 1960.

APPENDIX A

MAXIMUM AND MINIMUM RANGE TRAJECTORIES AND CONTROL HISTORIES

Graphs of the maximum and minimum range trajectories and associated control histories for the limiting values of entry flight-path angle at each of the several entry speeds employed are given on the following pages. The graphs for the steepest possible entry (i.e., a flight path angle of 180°) at an initial speed of 750 m/sec. are omitted because the range capability is merely 0.05°.

INDEX TO GRAPHS:

Initial Speed meters/sec	Initial Flight-Path Angle degrees	Max/Min Range	Page
750	90	Min	I-31
	90	Max	I-32
3500	90	Min	I-33
	90	Max	I-34
	110	Min	I-35
	110	Max	I-36
7833	90.5	Min	I-37
	90.5	Max	I-38
	101.75	Min	I-39
	101.75	Max	I-40
11080	94.71	Min	I-41
	94.71	Max	I-42
	99.8	Min	I-43
	99.8	Max	I-44

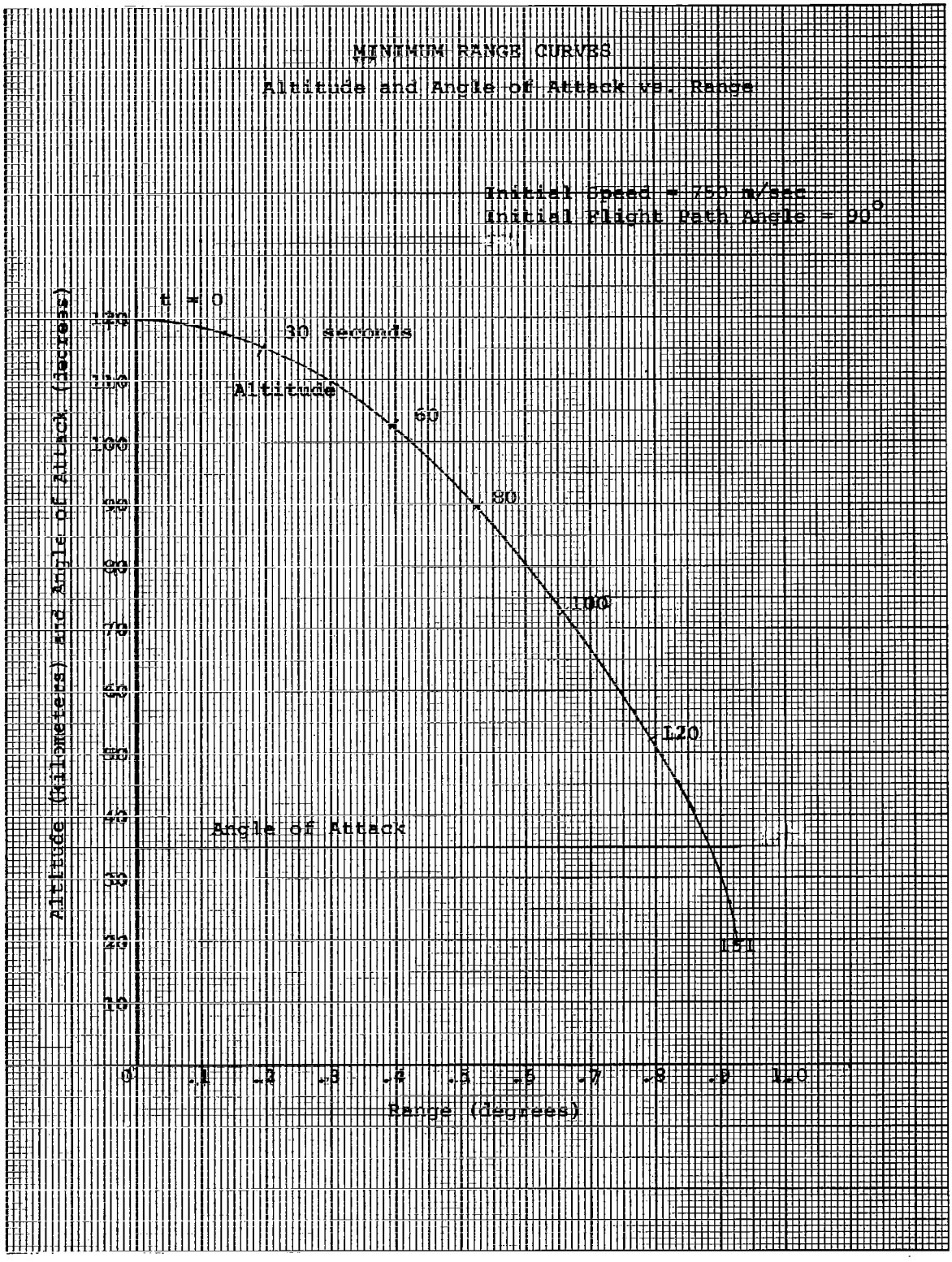
MINIMUM RANGE CURVES
Altitude and Angle of Attack vs. Range
Initial Speed = 750 m/sec
Initial Flight Path Angle = 90°
t = 0
30 seconds
Altitude
60
90
120
151
Angle of Attack
Altitude (Kilometers) and Angle of Attack (Degrees)
Range (Degrees)
0
.1
.2
.3
.4
.5
.6
.7
.8
.9
1.0

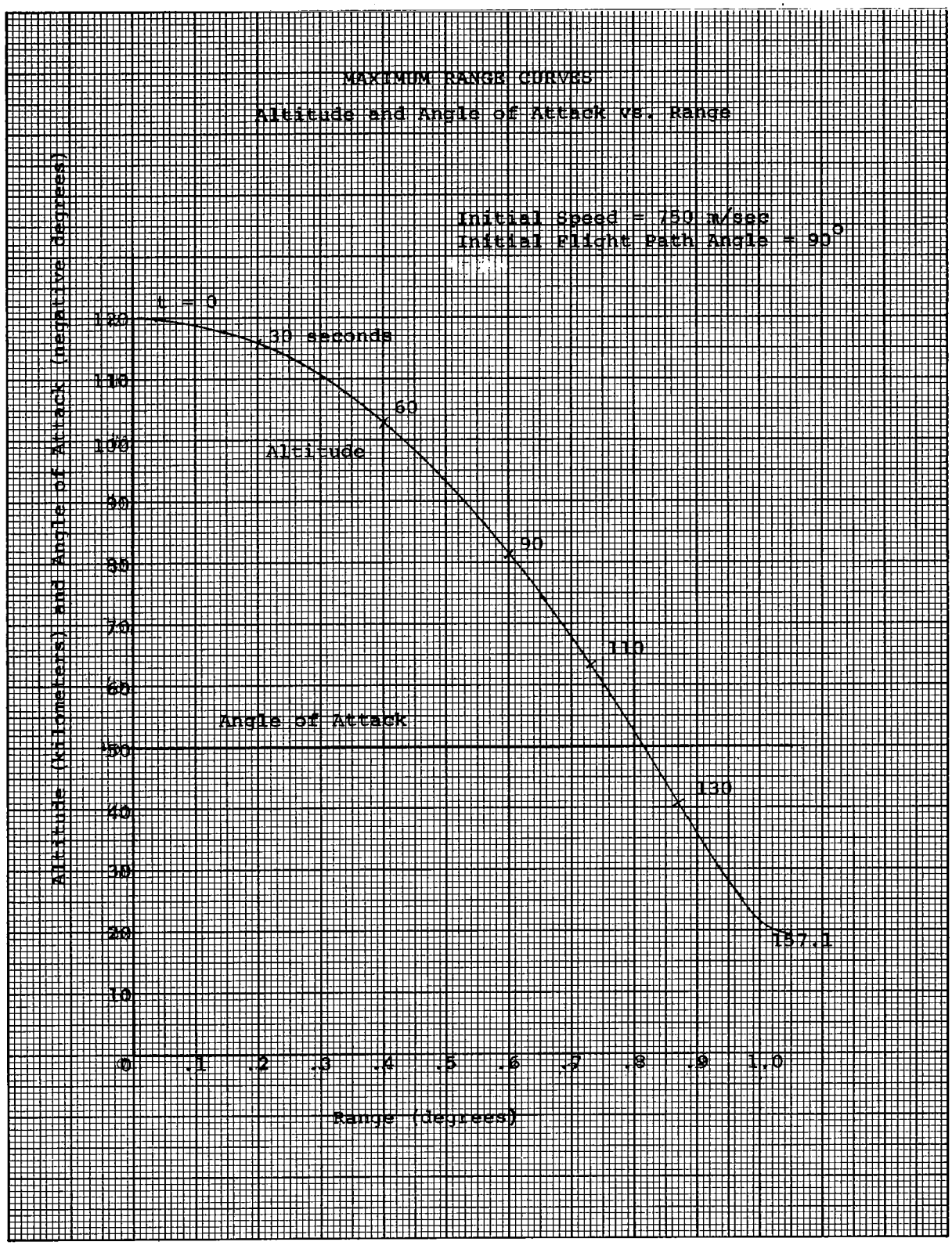
MAXIMUM RANGE CURVES
Altitude and Angle of Attack vs. Range
Initial Speed = 750 m/sec
Initial Flight Path Angle = 90°
t = 0
30 seconds
60
90
110
130
157.1
Altitude
Angle of Attack
Altitude (kilometers) and Angle of Attack (negative degrees)
120
110
100
90
80
70
60
50
40
30
20
10
0
.1
.2
.3
.4
.5
.6
.7
.8
.9
1.0
Range (degrees)

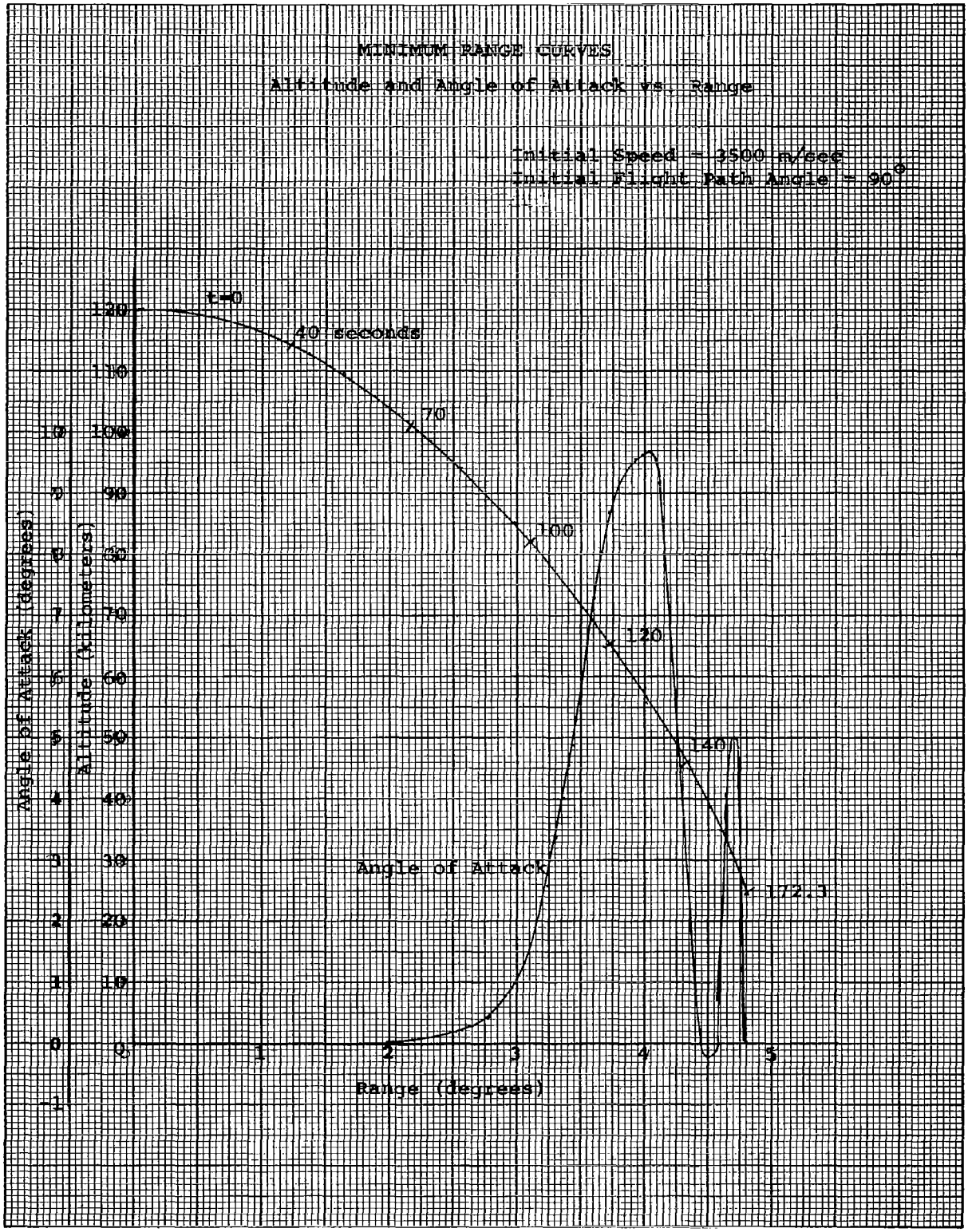
MINIMUM RANGE CURVES
Altitude and Angle of Attack vs. Range
Initial Speed = 3500 m/sec
Initial Flight Path Angle = 90°
t=0
40 seconds
70
100
120
140
172.3
Angle of Attack
Altitude (kilometers)
Angle of Attack (degrees)
Range (degrees)

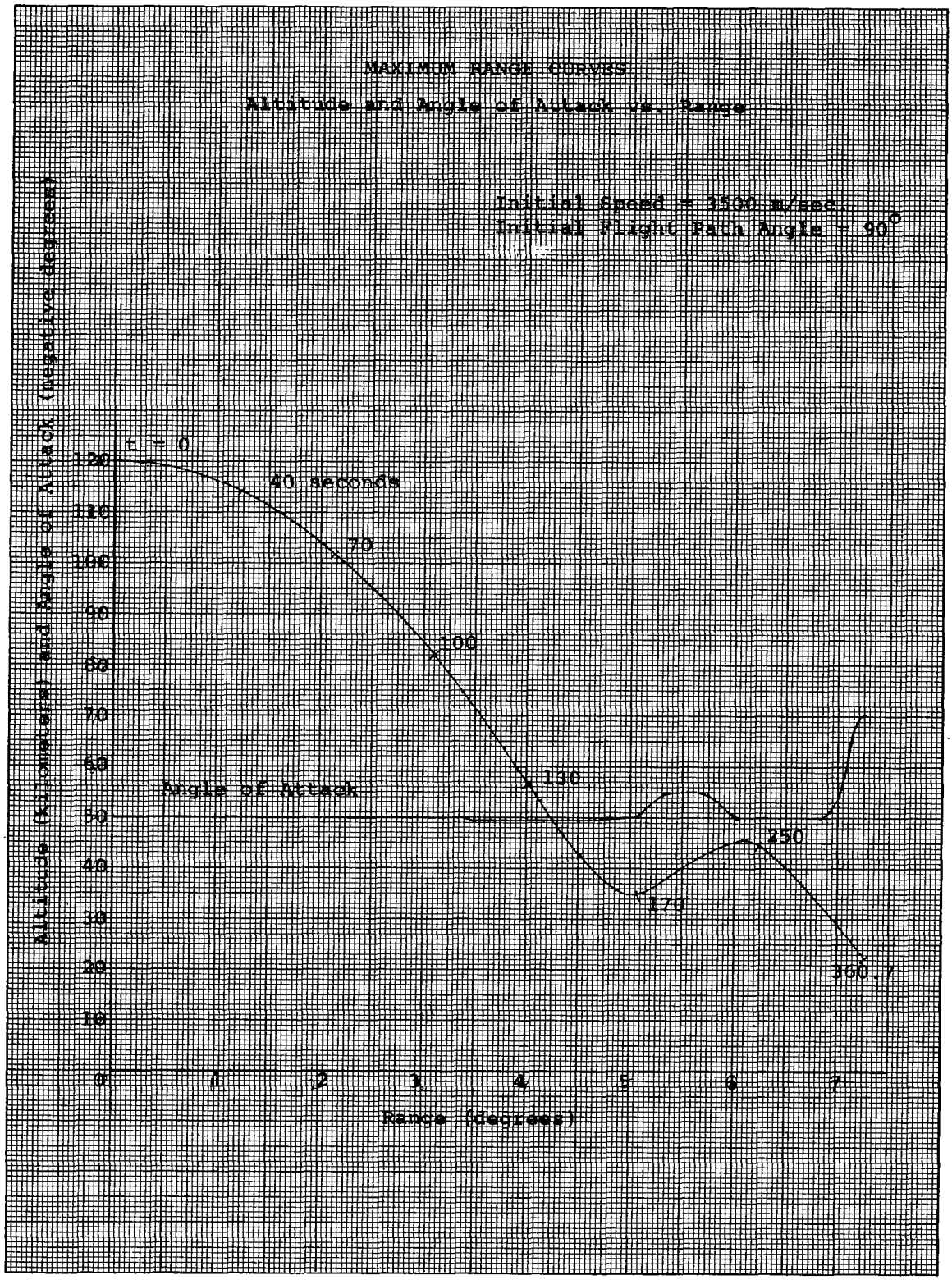
MAXIMUM RANGE CURVES
Altitude and Angle of Attack vs. Range
Initial Speed = 3500 m/sec.
Initial Flight Path Angle = 90°
Altitude (hundreds of meters) and Angle of Attack (hundreds of degrees)
t = 0
40 seconds
70
100
130
170
250
366.7
Angle of Attack
120
110
100
90
80
70
60
50
40
30
20
10
0
1
2
3
4
5
6
7
Range (degrees)

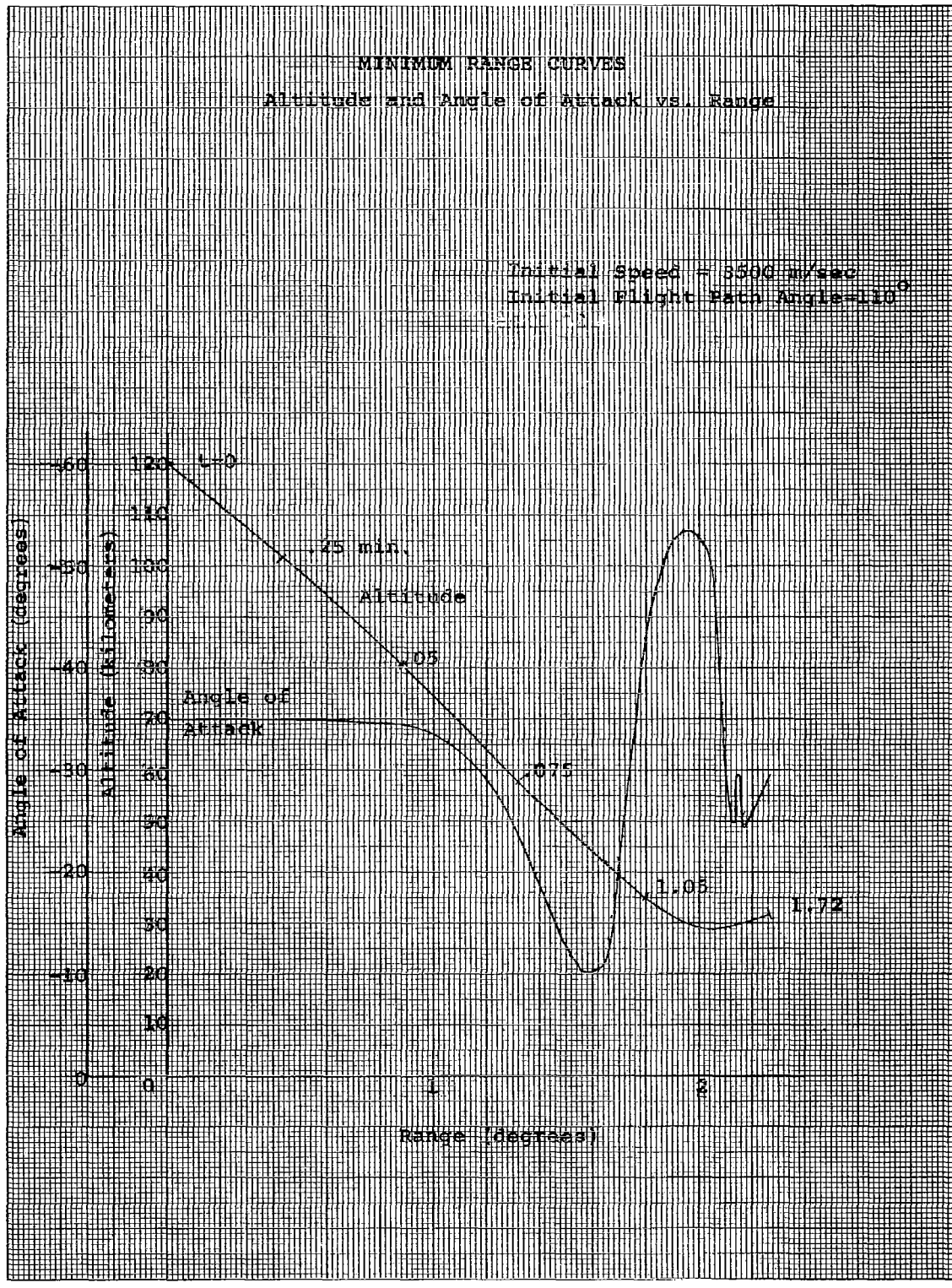
MINIMUM RANGE CURVES
Altitude and Angle of Attack vs. Range
Initial Speed = 3500 m/sec
Initial Flight Path Angle=-10°
t=0
.25 min.
.5
.75
1.05
1.72
Altitude
Angle of Attack
Angle of Attack (degrees)
Altitude (kilometers)
Range (degrees)
-60
-50
-40
-30
-20
-10
0
120
110
100
90
80
70
60
50
40
30
20
10
0
1
2

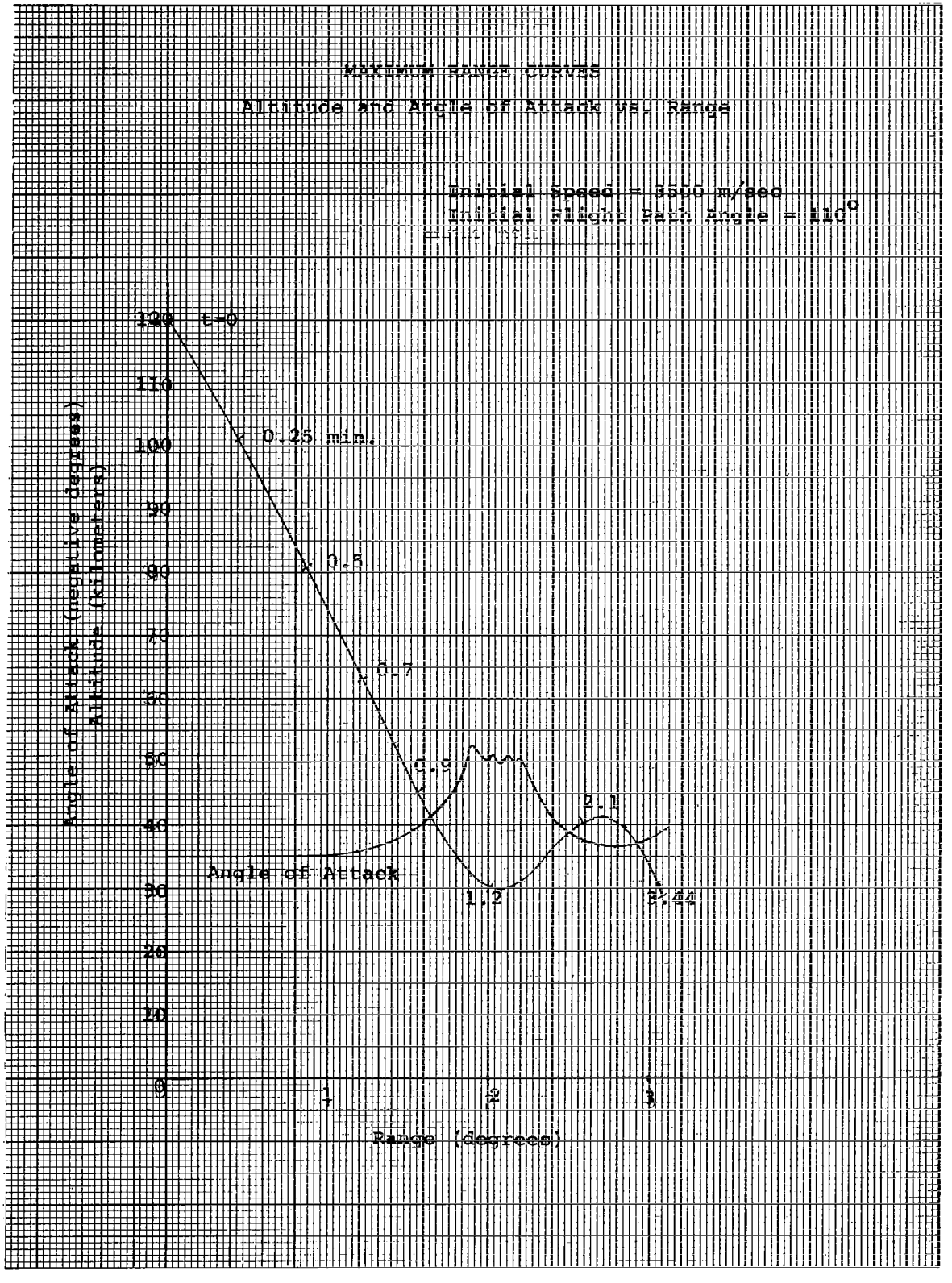
MAXIMUM RANGE CURVES
Altitude and Angle of Attack vs. Range
Initial Speed = 3000 m/sec
Initial Flight Path Angle = 30°
Angle of Attack (negative degrees)
Altitude (nautical miles)
120
110
100
90
80
70
60
50
40
30
20
10
0
t=0
0.25 min.
0.5
0.7
0.9
1.2
1.4
1.7
2.1
2.4 min
Angle of Attack
1
2
3
Range (degrees)

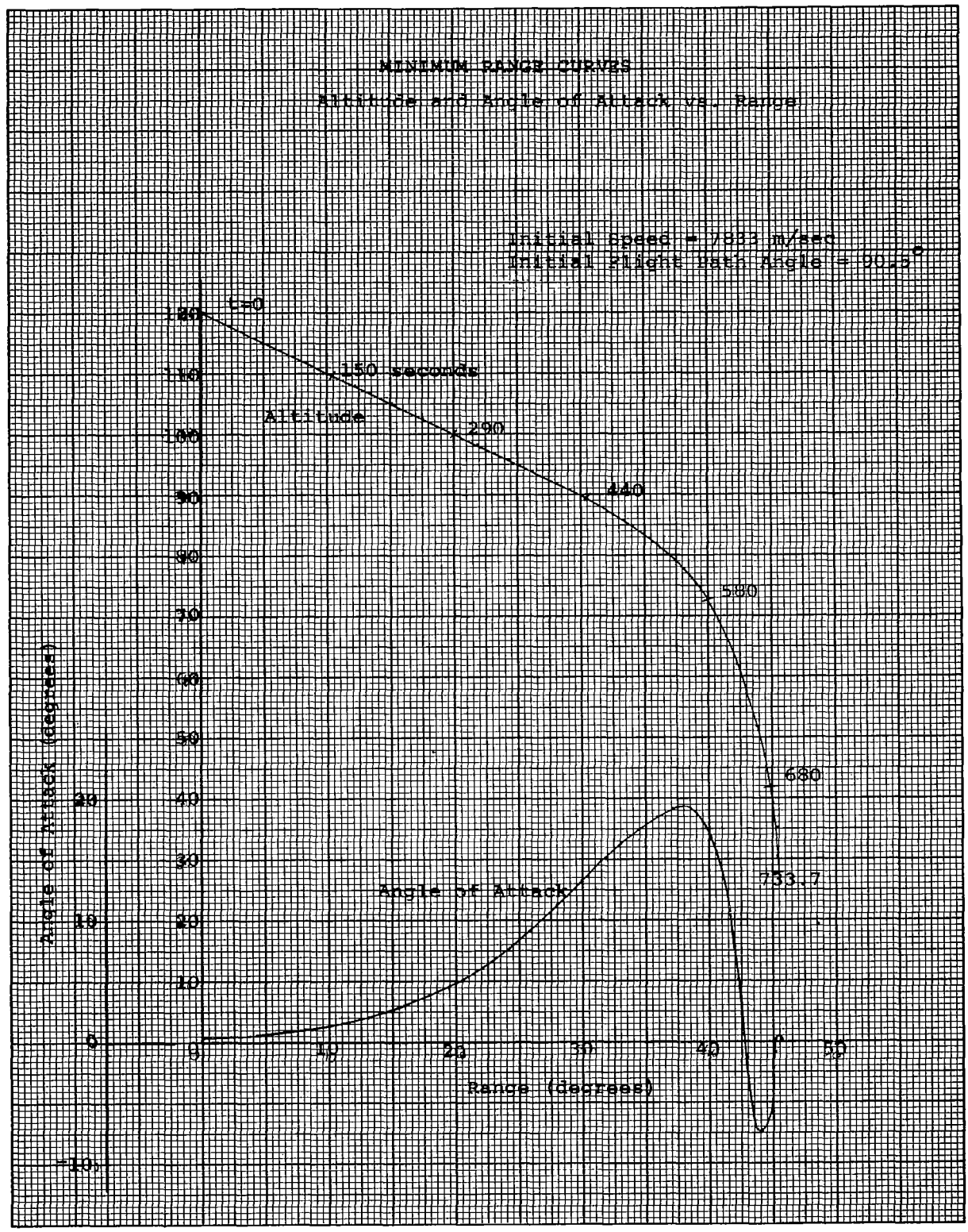
MINIMUM RANGE CURVES
Altitude and Angle of Attack vs. Range
Initial Speed = 7823 m/sec
Initial Flight Path Angle = 90.5°
t=0
150 seconds
Altitude
290
440
580
680
733.7
Angle of Attack
Angle of Attack (degrees)
Range (degrees)
0
10
20
30
40
50
-10

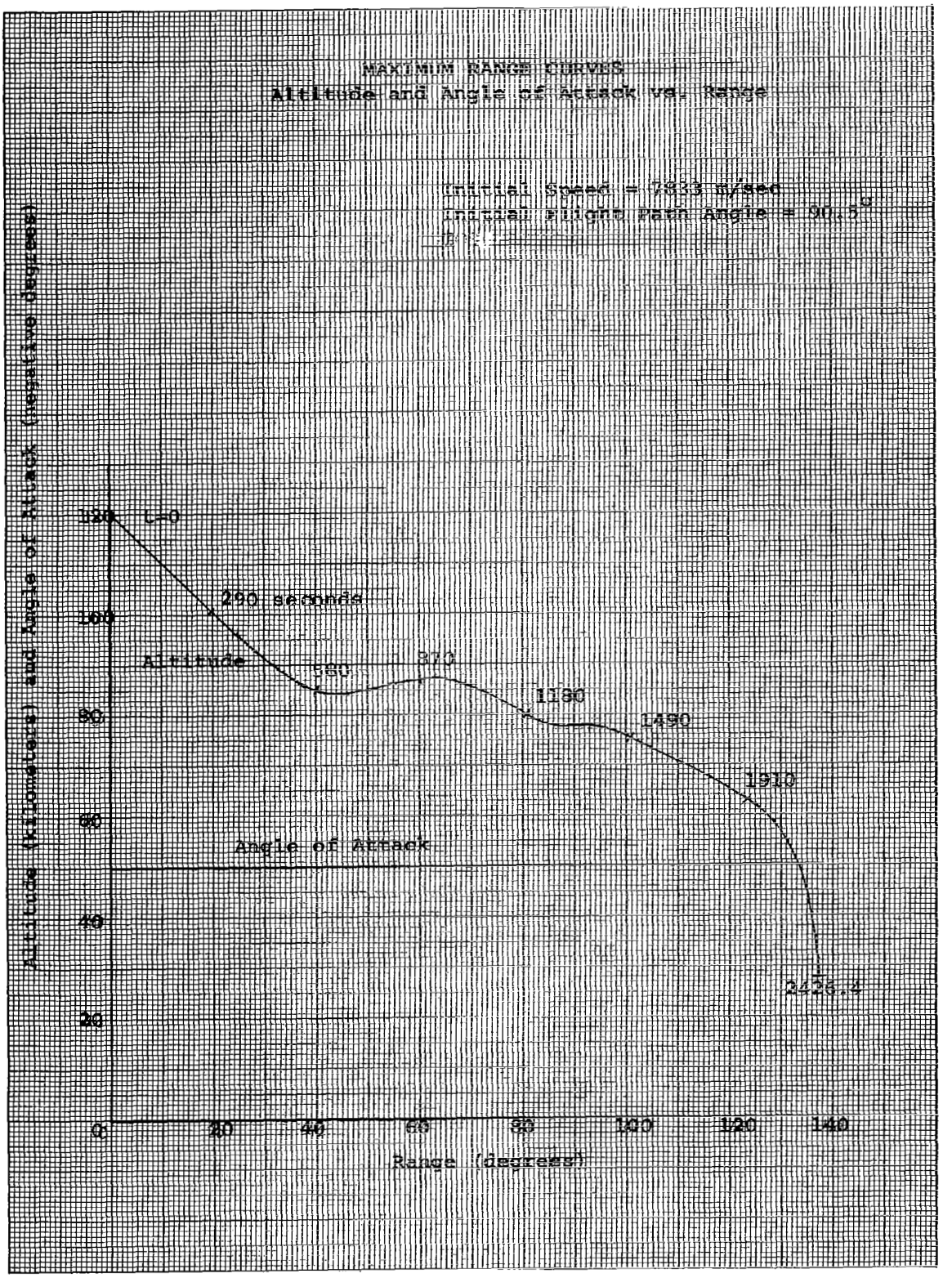
MAXIMUM RANGE CURVES
Altitude and Angle of Attack vs. Range
Initial Speed = 7833 m/sec
Initial Flight Path Angle = 90.5°
Altitude and Angle of Attack (negative degrees)
Altitude (kilometers)
320
L=0
290 seconds
100
Altitude
550
370
1180
80
1490
1910
60
Angle of Attack
40
2426.4
20
0
20
40
60
80
100
120
140
Range (degrees)

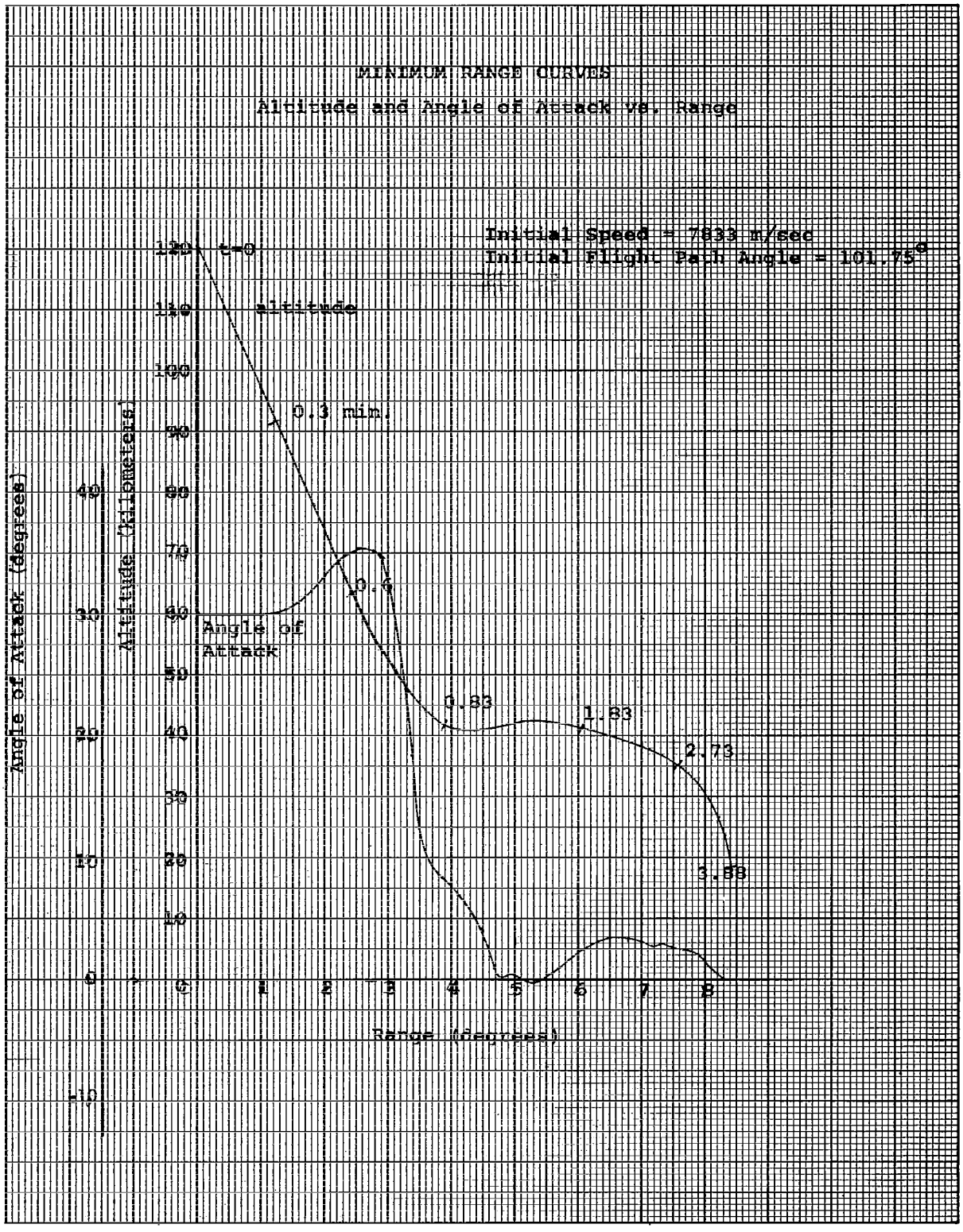
MINIMUM RANGE CURVES
Altitude and Angle of Attack vs. Range
Initial Speed = 7833 m/sec
Initial Flight Path Angle = 101.75°
t=0
altitude
0.3 min.
0.83
1.83
2.73
3.89
Angle of Attack
Altitude (kilometers)
Range (degrees)
Angle of Attack (degrees)

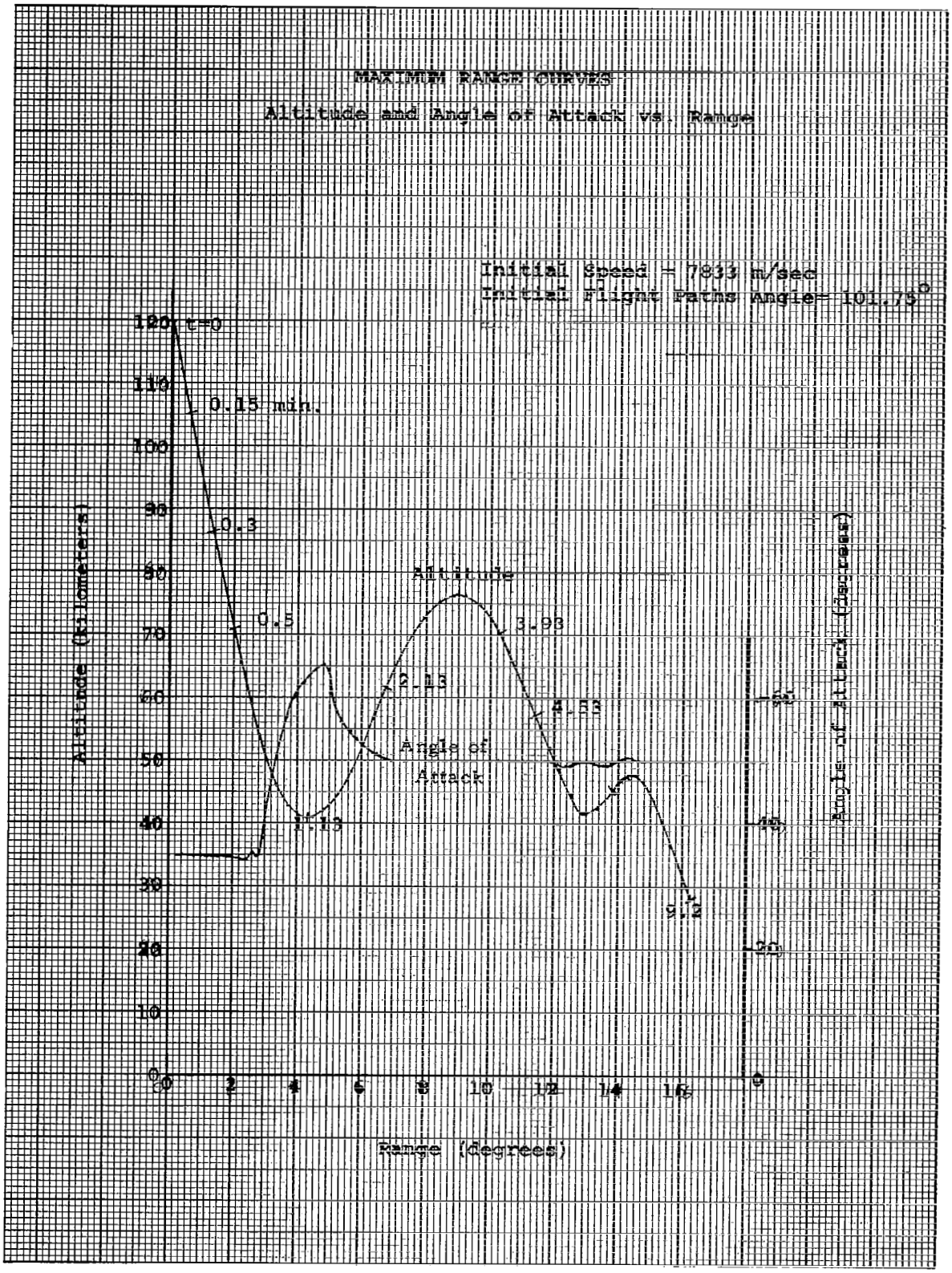
MAXIMUM RANGE CURVES
Altitude and Angle of Attack vs. Range
Initial Speed = 7833 m/sec
Initial Flight Path Angle= 101.75°
t=0
0.15 min.
0.3
0.5
Altitude
3.93
2.13
5.53
Angle of Attack
1.13
Altitude (Kilometers)
Angle of Attack (Degrees)
120
110
100
90
80
70
60
50
40
30
20
10
0
0
2
4
6
8
10
12
14
16
Range (Degrees)

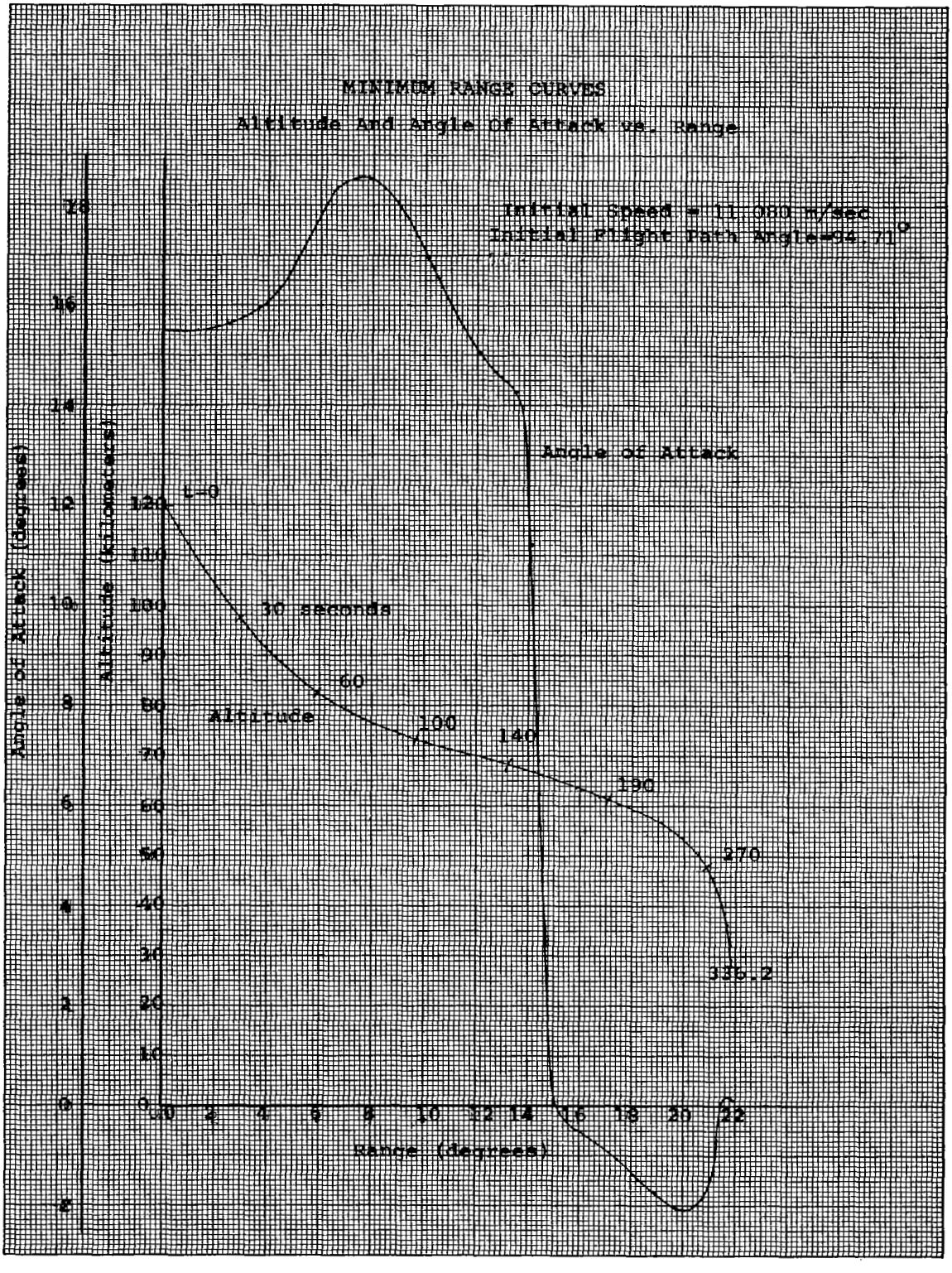
MINIMUM RANGE CURVES
Altitude and Angle of Attack vs. Range
Initial Speed = 11,080 m/sec
Initial Flight Path Angle=94.71°
Angle of Attack
t=0
30 seconds
60
100
140
190
270
336.2
Altitude
Angle of Attack (degrees)
Altitude (thousands of feet)
Range (degrees)

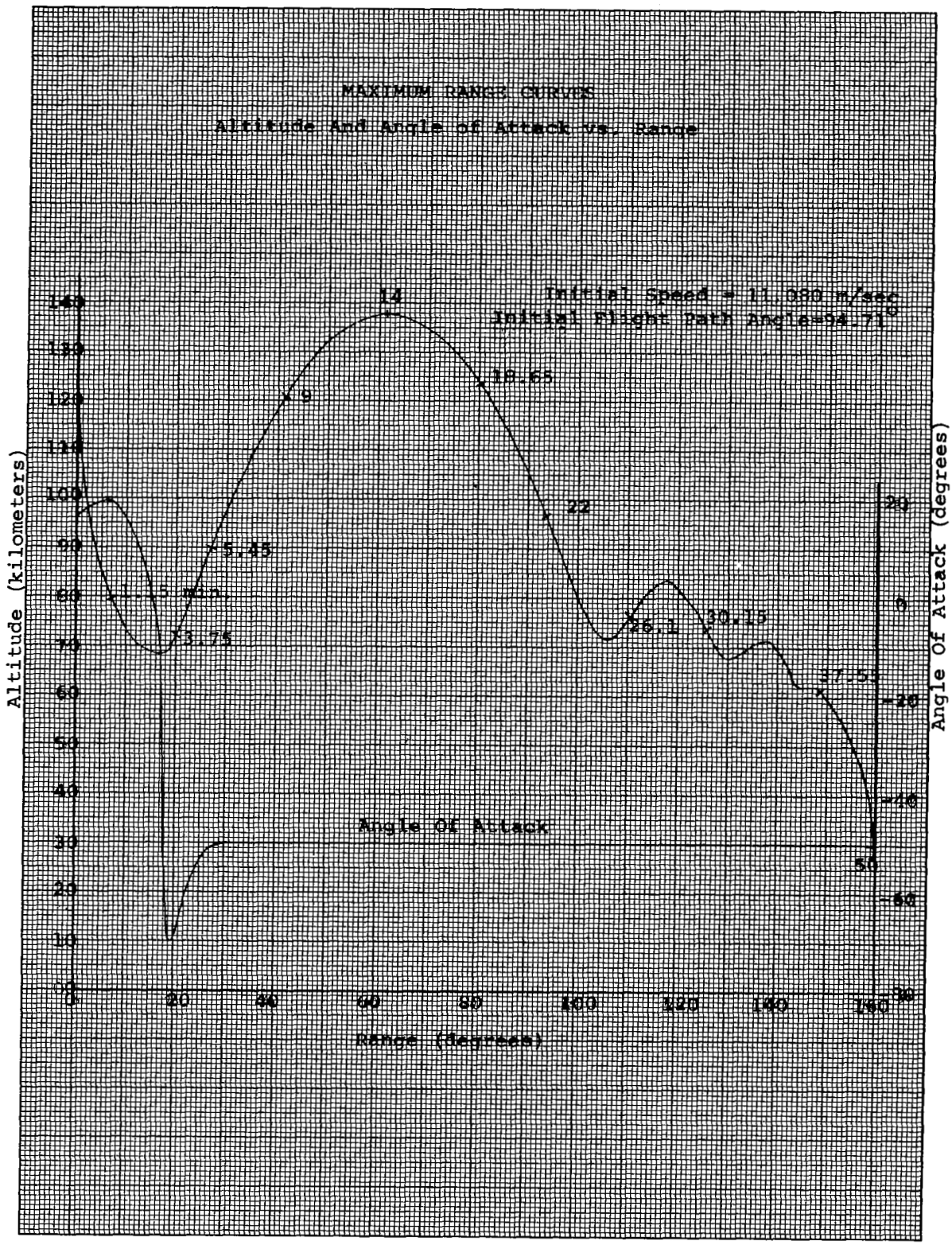
MAXIMUM RANGE CURVES
Altitude And Angle of Attack vs. Range
Initial Speed = 11,000 m/sec
Initial Flight Path Angle=94.71°
14
18.65
9
22
5.45
1.45
3.75
26.1
30.15
37.53
Altitude (kilometers)
Angle Of Attack (degrees)
Angle Of Attack
Range (degrees)
0
20
40
60
80
100
120
140
160
180
20
9
-20
-40
-60

MINIMUM RANGE CURVES
Altitude and Angle of Attack vs. Range
Initial Speed=11 000 m/sec
Initial Flight Path Angle=89.8°
Altitude
0.35 min.
0.7
1.3
2
3
4.709
Angle of Attack
Altitude (kilometers)
Angle of Attack (degrees)
Range (degrees)
*Computer program provided instantaneous switch between +70° and -70°. At both values $C_L = 0$ and $C_D = 0.34$

MAXIMUM RANGE CURVES
Altitude And Angle Of Attack vs. Range
Altitude
Initial Speed = 11,000 m/sec
Initial Flight Path Angle = 89.6°
Angle of Attack
Altitude (kilometers)
Angle of Attack (degrees)
Range (degrees)
7.5
12.22
15
17.23
20.43
26.63
27
32.2
4.28
2.13 minutes
t=0

PART II

EXO-ATMOSPHERIC ALTITUDE CEILINGS ON OPTIMUM RE-ENTRY TRAJECTORIES

1. SUMMARY

An upper bound on altitude is often a constraint included in re-entry optimization problems. For exo-atmospheric altitude ceilings imposed upon unpowered lifting vehicles, this requirement reduces to an inequality constraint on the dynamic state in which the vehicle leaves the atmosphere. The path is controlled within the atmosphere by varying the aerodynamic forces through the angle of attack and bank angle. The optimum control programs for this non-linear system are found using a high speed digital computer and the steepest-ascent method which generates a sequence of successively improved control histories. For an inverse-square gravitational field, an analytic expression is found relating the maximum skip altitude to the dynamic state of the vehicle at the edge of the atmosphere. This relation provides the information needed to define an intermediate point inequality constraint. The steepest-ascent mechanism then finds the optimum control programs during the entire time prior to departure from the atmosphere which ensures acceptable maximum skip altitude. An added bonus is the elimination of the need for numerical integration over the Keplerian ellipse for both the equations of motion and the adjoint equations. These analytic solutions result in a considerable saving in computer time if the skip-out is of long duration.

2. INTRODUCTION

Lifting vehicles re-entering the earth's atmosphere have some control over their descent trajectories. To find the "best" control programs for a given mission is the function of an optimization procedure. The steepest-ascent method begins with an arbitrary control program which in general is non-optimal and may not even bring the vehicle to the desired terminal state. It is, however, an iterative technique which generates a sequence of successively improved control programs. The measure of improvement is the increase in the pay-off and the correction of the terminal state.

One constraint often included in the problem of optimizing re-entry trajectories is an altitude ceiling. A maximum altitude is prescribed apriori and the vehicle must not exceed it either during the entire flight or during a specified portion of it. A technique, which has been incorporated into the steepest-ascent method, to satisfy this condition is the altitude penalty function.

A simple way to do this is to compute the area in the altitude versus time graph which lies above the specified maximum altitude for each non-optimal trajectory. This area is included as a terminal constraint. The condition that this violation vanish is then added to those which determine the corrections to the control program. The altitude violation is removed by the time the optimal trajectory is found. For altitude ceilings which lie inside the atmosphere, the altitude penalty function was satisfactory, although the process did not converge as rapidly as the more direct method of instantaneous inequality constraints, recently developed at Raytheon and presented in References 2 and 3.

The penalty function method proved difficult to apply to maximum range problems for vehicles entering the atmosphere at escape speeds and subject to altitude ceilings outside the atmosphere. The skip altitude is extremely sensitive to small changes in the dynamic state of the vehicle as it leaves the atmosphere. Another method was needed for these problems.

The exo-atmospheric portion of the path of an unpowered vehicle is completely determined by its dynamic state as it leaves the atmosphere. For a spherical earth, an analytic expression can be found which relates the maximum skip altitude to the velocity at the edge of the atmosphere. This condition permits the inclusion in the computer program of an intermediate point inequality constraint. It is treated in the same way as a terminal constraint except that its influence function is calculated only from the initial time until the time the vehicle leaves the atmosphere. The control program is altered during this time period in such a way that the pay-off and the terminal constraints are improved subject to the additional condition that the vehicle exit the atmosphere with a velocity which ensures acceptable maximum altitude. This constraint is then dropped from the system and plays no part in changes made to the remainder of the control program. This method is more direct than the penalty function approach and should be used in high speed re-entry problems.

3. LIST OF SYMBOLS

C_D	drag coefficient
C_L	lift coefficient
E	energy divided by m/2
F	matrix of partial derivatives $\frac{\partial f_i}{\partial x_j}$
G	" " " " $\frac{\partial f_i}{\partial \alpha_j}$
$I_{\Psi\Psi}$, $I_{\Psi\Phi}$, $I_{\Phi\Phi}$	integrals used in steepest-ascent procedure see equation (19)
R_E	earth radius
S	vehicle reference area
T	trajectory final time
V_T	total speed
W	weighting matrix in steepest-ascent procedure
$(dP)^2$	mean square perturbation of the control variable programs
e	eccentricity of Keplerian ellipse
f_i	function in equations of motion, see equation (1)
h	angular momentum
$\underline{i}_\zeta$, $\underline{i}_\eta$, $\underline{i}_\xi$	right hand vector triad used in Keplerian Analysis
m	vehicle mass
r	radial distance of vehicle from center of earth
r_A	radius of edge of atmosphere
r_{MAX}	prescribed radius to altitude ceiling
$\underline{r}$	radius vector of vehicle

$\underline{r}_o$ initial radius vector in Keplerian Analysis

$\dot{\underline{r}}$ velocity vector of vehicle

t time

t_o initial time

u, v, w spherical velocity components of vehicle

$\underline{v}_o$ initial velocity vector in Keplerian Analysis

x_i a state variable

$\underline{x}$ state variable vector

Φ pay off function

$\frac{\partial \Phi}{\partial \underline{x}} = \left[\frac{\partial \Phi}{\partial x_1}, \frac{\partial \Phi}{\partial x_2}, \ldots \frac{\partial \Phi}{\partial x_n} \right]$ evaluated at T

Ψ_k a terminal constraint

Ψ_p terminal constraint used to determine T

Ψ vector of terminal constraints

$\frac{\partial \Psi}{\partial \underline{x}}$ matrix of partial derivatives $\frac{\partial \Psi_i}{\partial x_j}$

Ω_e angular velocity of earth

α angle of attack

$\underline{\alpha}$ vector of control variables

$\underline{\alpha}_o$ nominal vector of control variables

ξ, η, ζ coordinate system used in Keplerian Analysis

θ co-latitude of vehicle

$\underline{\lambda}(t)$ solution of adjoint system of differential equations

$\underline{\lambda}_\Phi$ influence function vector for pay-off

$\underline{\lambda}_{\Psi_k}$ " " " " k^{th} terminal constraint

Λ_{Ψ} influence function matrix for terminal constraints

μ constant in steepest-ascent procedure, see equation (16) and (17)

μ_e gravitational constant

$\underline{\nu}$ vector of constants in steepest-ascent procedure, see equation (16) and (17)

ρ air density

σ bank angle

ϕ longitude angle

Subscripts 1, 2, 3 on state variables u, v, w, r, θ, ϕ, and time T indicate critical points on the Keplerian ellipse portion of the trajectory. 1 is the point at which the vehicle leaves the atmosphere, 2 the point of maximum altitude and 3 the point of atmosphere re-entry.

4. MATHEMATICAL MODEL

The vehicle is a mass particle acted upon by the inverse square gravitational field of the earth and in addition, when in the atmosphere by its lift and drag forces. The control functions are angle of attack and bank angle which modulate the aerodynamic forces. The motion is described in a spherical coordinate system concentric with a spherical rotating earth of radius R_E, which is enveloped by an 1962 U.S. model atmosphere. The "edge of the atmosphere" is defined as a sphere of radius r_A. The numerical value of r_A is chosen with the vehicle characteristics and entry speed in mind so that the aerodynamic forces are negligible at this altitude and the model is continuous. The coordinate system is shown in Figure 1.

Coordinate System

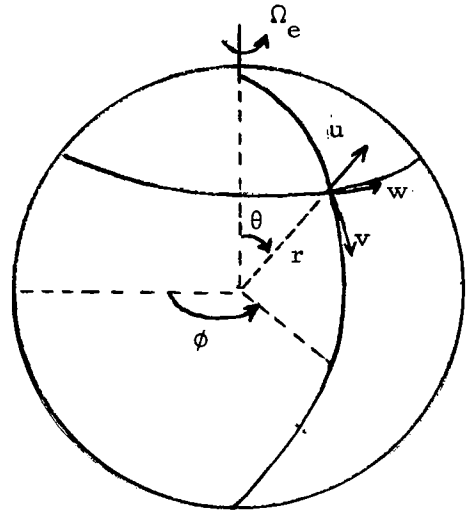

Figure 1

The equations of motion are:

$$\dot{u} = \frac{v^2 + w^2}{r} + r\,\Omega_e{}^2 \sin^2\theta + 2\,\Omega_e\, w \sin\theta$$

$$+ \frac{\rho\, S V_T}{2\, m} \left[- u\, C_D + C_L \sqrt{v^2 + w^2} \cos\sigma \right] - \frac{\mu_e}{r^2}$$

$$\dot{v} = -\frac{u\,v}{r} + \frac{w^2 \cot\theta}{r} + r\,\Omega_e^{\,2} \cos\theta \sin\theta + 2\,\Omega_e\, w \cos\theta$$

$$- \frac{\rho\, S V_T}{2\,m} \left[v\, C_D + \frac{u\,v\,C_L \cos\sigma + w\, C_L\, V_T \sin\sigma}{\sqrt{v^2 + w^2}} \right]$$

$$\dot{w} = -\frac{u\,w}{r} - \frac{v\,w \cot\theta}{r} - 2\,\Omega_e\,(u \sin\theta + v \cos\theta)$$

$$- \frac{\rho\, S V_T}{2\,m} \left[w\, C_D + \frac{u\,w\,C_L \cos\sigma - v\, C_L\, V_T \sin\sigma}{\sqrt{v^2 + w^2}} \right]$$

$$\dot{r} = u$$

$$\dot{\theta} = \frac{v}{r}$$

$$\dot{\phi} = \frac{w}{r \sin\theta}$$

5. OPTIMIZATION PROCEDURE

A vehicle entering the earth's atmosphere with arbitrary control programs and initial conditions will have a trajectory belonging to one of four classes. These are shown in Figure 2.

Types of Re-Entry Trajectories

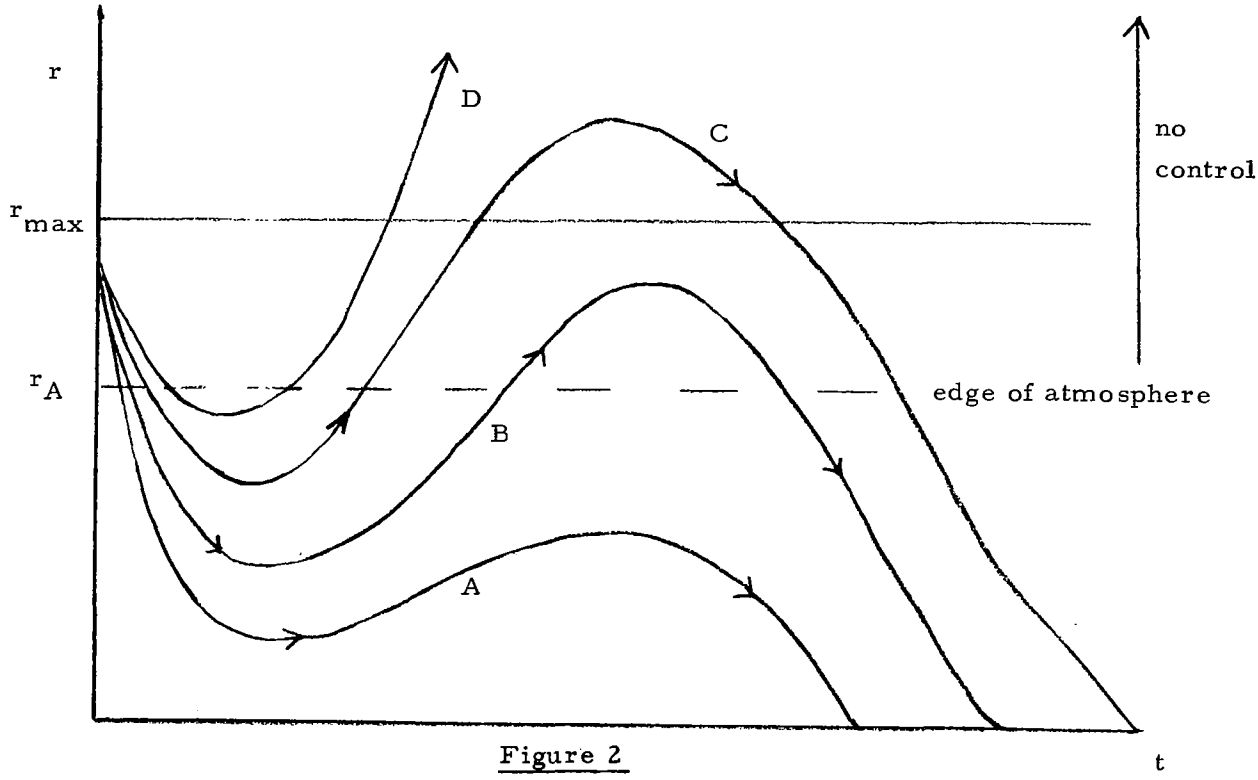

Figure 2

The path labelled A has no exo-atmospheric segment after the initial penetration of the atmosphere. It satisfies the altitude constraint and can be optimized using the steepest-ascent procedure which is summarized in Section 5.1.

The path labelled B is also satisfactory and will be optimized in the same way as path A except numerical integration will be suspended during the skip-out phase. The re-entry state will be computed from the exit state using analytic solutions of the two body problem. The inclusion of these solutions in the optimization procedure is shown in Section 5.2 while the solutions themselves are listed in Section 6.

The path labelled C violates the altitude ceiling and the steepest-ascent procedure for altering the control programs must now include the intermediate point constraint on the dynamic state in which the vehicle leaves the atmosphere. This addition is explained in Section 5.3 Numerical integration will again be suspended for the exo-atmospheric portion of the trajectory and replaced by the analytic solutions.

The path labelled D is an escape trajectory. The steepest-ascent procedure may succeed in converting this path to a return one. Section 5.4 indicates how this may be done.

5.1 Steepest-Ascent Optimization Procedure

This section is a summary of the mathematical tool used to find an optimum trajectory. It is described in detail in Reference 1. This discussion is included so that the use of an intermediate point constraint to satisfy an exo-atmospheric altitude ceiling may be understood.

The motion of the vehicle is described by the set of non-linear differential equations given in Section 4. These equations contain the unspecified control functions angle of attack α (t) and bank angle, σ (t) . The problem is to find the control histories which bring the vehicle to the terminal time, T, in such a dynamic state that a given function of the terminal state Φ , called the pay-off, is maximized and given functions $\Psi_k = 0$ for $k = 1, 2, \cdots p$, called terminal constraints, are satisfied.

The steepest-ascent procedure requires that the engineer choose "reasonable" control functions α_o (t) and σ_o (t) defined over the interval $[\ t_o, T\ ]$ in order to start the iterative process. Using these nominal control programs and the given initial values of the state variables, the equations of motion are integrated numerically from t_o to T, which is determined by one of the terminal constraints, say $\Psi_p = 0$. This stopping condition of the numerical integration can be any of the terminal constraints provided $\dot{\Psi}_p$ (T) $\neq 0$. The resulting trajectory will not, in general, maximize Φ nor satisfy any $\Psi_k = 0$ except the pth one. It is now necessary to compute changes in the control functions, $\delta\alpha$ (t) and $\delta\sigma$ (t) so that the next pair of controls: α_1 (t) = α_o (t) + $\delta\alpha$ (t) and σ_1 (t) = σ_o (t) + $\delta\sigma$ (t) will produce a <u>better</u> trajectory. The criterion which determines the changes in the control programs is the <u>maximization</u> of the <u>change</u>

in pay-off, subject to specified changes in the terminal constraints for a specified mean square perturbation of the control functions. The calculations are based on "small" perturbations about a nominal path. The amount of change in the control programs which is justified, i.e., which will produce the effect predicted by the linear theory, is limited. Thus, the process must be repeated until no changes in the controls result: $\delta\, a\,(t) = \delta\, \sigma\,(t) \equiv 0$.

The expressions for the changes in the control are derived here. Let $\underline{x}\,(t)$ be the n dimensional vector of state variables, $\underline{a}\,(t)$ be the m dimensional vector of control variables. The differential equations of motion are:

$$\dot{x}_i = f_i\,(x_1, x_2 \cdots x_n, a_1, a_2, \cdots a_m, t)$$
$$i = 1, 2, \cdots n. \qquad (1)$$

Let F be the nxn matrix with general element $\dfrac{\partial f_i}{\partial x_j}$ and

G be the nxm matrix with general element $\dfrac{\partial f_i}{\partial a_j}$ with

all partial derivatives evaluated on the nominal trajectory.

Because we are concerned with changing terminal quantities, Φ and Ψ_k, we need expressions which relate changes in terminal conditions to changes in the entire control histories. These can be found by considering small perturbations about the nominal path. From Equation (1) we have:

$$\delta\, \dot{\underline{x}} = \frac{d}{dt}\, \underline{\delta\, x} = F\, \underline{\delta\, x} + G\, \underline{\delta\, a} \qquad (2)$$

If we define an n dimensional vector $\underline{\lambda}\,(t)$ as one which satisfies the set of adjoint differential equations:

$$\dot{\underline{\lambda}}\,(t) = -F'\, \underline{\lambda}\,(t) \qquad (3)$$

Where $'$ means transposed matrix, we can combine equations (2) and (3) to give:

$$\frac{d}{dt}\left(\underline{\lambda}' \underline{\delta x}\right) = \underline{\lambda}' G \underline{\delta \alpha} \tag{4}$$

Integrating this equation from t_o to T and assuming for simplicity* that the initial state is fixed so that $\underline{\delta x}(t_o) = 0$, we have:

$$\underline{\lambda}'(T)\,\underline{\delta x}(T) = \int_{t_o}^{T} \underline{\lambda}' G \underline{\delta \alpha}\, dt \tag{5}$$

Here we have an expression which relates changes in terminal conditions to changes in the entire control history. We need to relate this to changes in the pay-off and terminal constraints. With this in mind, we seek expressions for $d\Phi$ and $d\Psi_k$. We know:

$$\Phi = \Phi(x_1(T),\ x_2(T),\ \cdots x_n(T))$$

and so

$$d\Phi = \sum_{j=1}^{n} \left.\frac{\partial \Phi}{\partial x_j}\right|_T \underline{\delta x_j}(T) + \dot{\Phi}\, dT \tag{6}$$

where $|_T$ means the partial derivative is evaluated at T. In the same way:

$$d\Psi_k = \sum_{j=1}^{n} \left.\frac{\partial \Psi_k}{\partial x_j}\right|_T \underline{\delta x_j}(T) + \dot{\Psi}_k\, dT, \quad k = 1, 2, \cdots, p. \tag{7}$$

But, since $\Psi_p = 0$ is the stopping condition for the numerical integration and is always satisfied, we choose $d\Psi_p = 0$. Thus:

$$dT = -\frac{1}{\dot{\Psi}_p} \sum_{j=1}^{n} \left.\frac{\partial \Psi_k}{\partial x_j}\right|_T \underline{\delta x_j}(T) \tag{8}$$

* Reference 1 provides the derivation without this assumption. It is made here merely for the sake of clarity.

In order to simplify the notation, let $\frac{\partial \Phi}{\partial \underline{x}}$ represent an n dimensional row vector with ith element $\frac{\partial \Phi}{\partial x_i}\Big|_T$ and let $\frac{\partial \Psi}{\partial \underline{x}}$ be a (p-1) x n matrix with general term $\frac{\partial \Psi_i}{\partial x_j}\Big|_T$. Replacing d T in Equations (6) and (7) by its value given in Equation (8), we have:

$$d\Phi = \left(\frac{\partial \Phi}{\partial \underline{x}} - \frac{\dot{\Phi}}{\dot{\Psi}_p} \frac{\partial \Psi_p}{\partial \underline{x}} \right) \underline{\delta x}\ (T) \tag{9}$$

$$d\Psi = \left(\frac{\partial \Psi}{\partial \underline{x}} - \frac{\dot{\Psi}}{\dot{\Psi}_p} \frac{\partial \Psi_p}{\partial \underline{x}} \right) \underline{\delta x}\ (T) \tag{10}$$

where Ψ is a (p-1) dimensional vector with ith element Ψ_i. Now we can use Equations (9), (10) and (5) to relate $d\Phi$ and $d\Psi$ to $\underline{\delta a}$.

We define influence functions which are p n dimensional vectors, $\underline{\lambda}_\Phi$ (t), $\underline{\lambda}_{\Psi_k}$ (t) for $k = 1, 2, \ldots, p-1$. each of which satisfies the adjoint differential equations and whose numerical value for $t = T$ is given by:

$$\underline{\lambda}_\Phi (T) = \frac{\partial \Phi}{\partial \underline{x}} - \frac{\dot{\Phi}}{\dot{\Psi}_p} \frac{\partial \Psi_p}{\partial \underline{x}} \tag{11}$$

$$\underline{\lambda}_{\Psi_k} (T) = \frac{\partial \Psi_k}{\partial \underline{x}} - \frac{\dot{\Psi}_k}{\dot{\Psi}_p} \frac{\partial \Psi_p}{\partial \underline{x}} \tag{12}$$

Let Λ_Ψ (t) be the n x p-1 matrix with general column $\underline{\lambda}_{\Psi_k}$ (t).

Combining equations (11), (12), (9), (10) and (5) we have:

$$d\Phi = \underline{\lambda}'_\Phi (T)\ \underline{\delta x}\ (T) = \int_{t_o}^{T} \underline{\lambda}'_\Phi G\ \underline{\delta a}\ dt \tag{13}$$

$$d\Psi = \Lambda'_\Psi (T)\ \underline{\delta x}\ (T) = \int_{t_o}^{T} \Lambda'_\Psi G\ \underline{\delta a}\ dt \tag{14}$$

We can now apply the criterion of the steepest-ascent procedure. We seek changes in the control functions $\underline{\delta\alpha}$ which will maximize the change in pay-off, $d\Phi$ for specified changes in the terminal constraints $d\Psi$ and for a specified mean square perturbation of the control function defined by:

$$(dP)^2 = \int_{t_o}^{T} \underline{\delta\alpha}' \, W \, \underline{\delta\alpha} \, dt \tag{15}$$

Where W is a weighting matrix chosen by the engineer. To do this, we form, from Equations (13), (14), and (15), the linear combination:

$$d\Phi = \int_{t_o}^{T} \underline{\lambda}'_{\Phi} \, G \, \underline{\delta\alpha} \, dt + \underline{\nu}' \left[d\Psi - \int_{t_o}^{T} \Lambda'_{\Psi} \, G \, \underline{\delta\alpha} \, dt \right]$$

$$+ \mu \left[(dP)^2 - \int_{t_o}^{T} \underline{\delta\alpha}' \, W \, \underline{\delta\alpha} \, dt \right] \tag{16}$$

or, combining the integrals:

$$d\Phi = \int_{t_o}^{T} (\underline{\lambda}'_{\Phi} \, G - \underline{\nu} \Lambda'_{\Psi} \, G - \mu \, \underline{\delta\alpha}' \, W) \, \underline{\delta\alpha} \, dt$$

$$+ \underline{\nu}' \, d\Psi + \mu \, (dP)^2 \tag{17}$$

Where $\underline{\nu}$ is a p-1 dimensional vector of unknown constants and μ is an unknown constant. To maximize $d\Phi$, we set its variation with respect to the control function to zero. Using Equation (17) for this and coupling it with Equations (14) and (15), we find the constants $\underline{\nu}$ and μ and

$$\underline{\delta\alpha}(t) = W^{-1} G' (\underline{\lambda}_{\Phi} - \Lambda_{\Psi} I^{-1}_{\Psi\Psi} I_{\Phi}) \sqrt{\frac{(dP)^2 - d\Psi' I^{-1}_{\Psi\Psi} d\Psi}{I_{\Phi\Phi} - I_{\Phi\Phi} I^{-1}_{\Psi\Psi} I_{\Psi\Phi}}}$$

$$+ W^{-1} G' \Lambda_{\Psi} I^{-1}_{\Psi\Psi} d\Psi \tag{18}$$

where $$I_{\Psi\Psi} = \int_{t_o}^{T} \Lambda'_{\Psi} \; G \; W^{-1} G' \; \Lambda_{\Psi} \; dt$$

$$I_{\Psi\Phi} = \int_{t_o}^{T} \Lambda'_{\Psi} \; G \; W^{-1} G' \; \underline{\lambda}_{\Phi} \; dt$$

$$I_{\Phi\Phi} = \int_{t_o}^{T} \underline{\lambda}'_{\Phi} \; G \; W^{-1} G' \; \underline{\lambda}_{\Phi} \; dt \qquad (19)$$

Thus, the next control program, $\underline{\alpha}_1(t) = \underline{\alpha}_0(t) + \underline{\delta\alpha}(t)$, will produce a trajectory with terminal conditions which have been changed by the requested amount $d\Psi$ and with maximum possible increase in the pay-off provided the "amount" of specified control variable change measured by $(dP)^2$ is not so large that the small perturbation theory used is invalid or the requested changes $d\Psi$ are larger than can be achieved with this $(dP)^2$ which is indicated by the term in the square root of Equation (18) being negative. The procedure is then repeated replacing $\alpha_o(t)$ by $\alpha_1(t)$. The iterations terminate when $\alpha_{n+1}(t) = \alpha_n(t)$.

This process is summarized in Figure 3, Steepest-Ascent Optimization Procedure, Flow Chart A for a class A re-entry trajectory. This class includes all trajectories which remain in the atmosphere after initial penetration. Thus $r = r_A$ shortly after t_o and never again. Trajectories of the types labelled B, C and D in Figure 2 arrive at r_A at least once more and so the condition that $r \neq r_A$ a second time is satisfied only by class A trajectories.

Steepest-Ascent Optimization Procedure

Flow Chart A

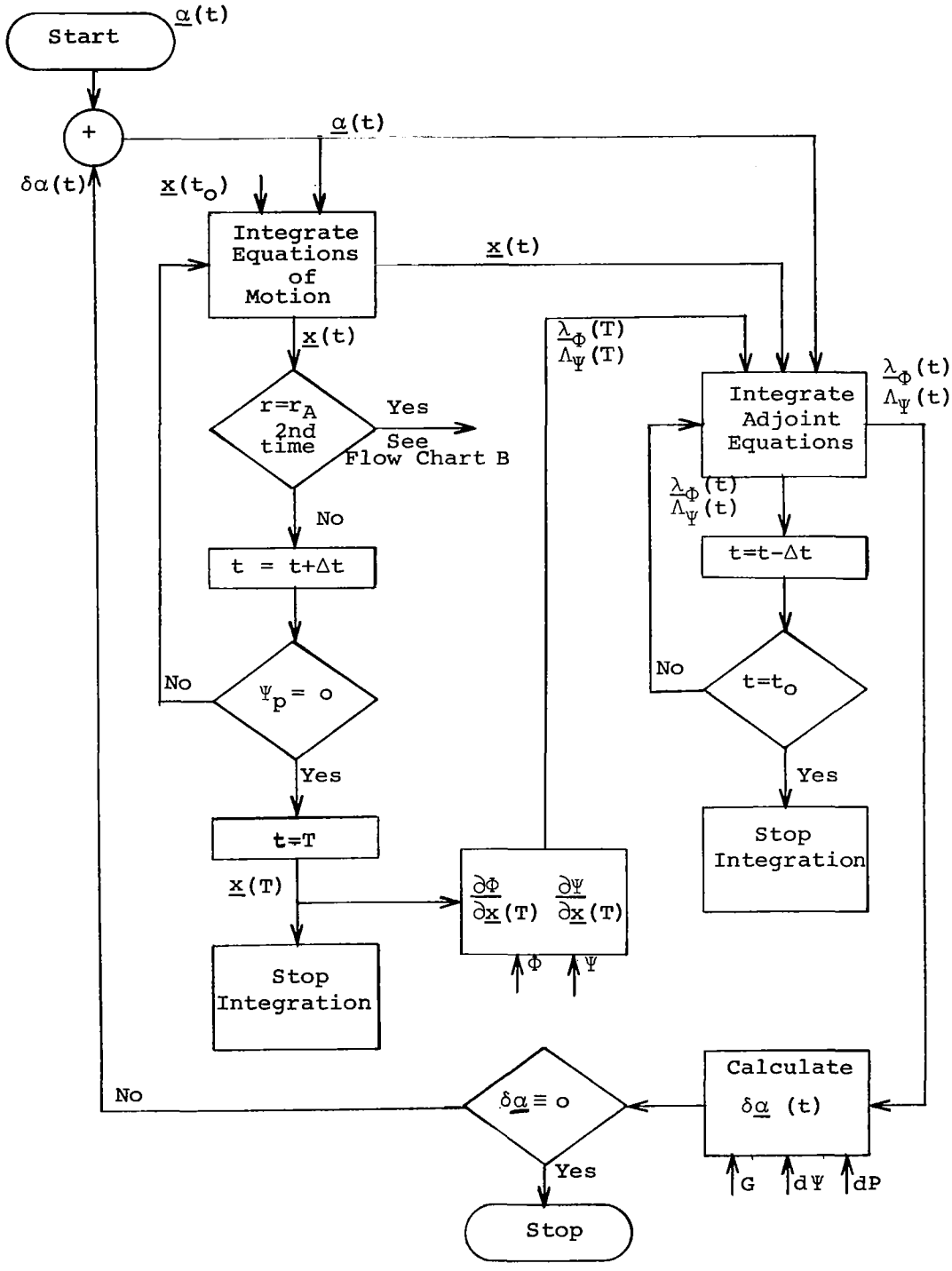

Figure 3

5.2 SATISFACTORY SKIP TRAJECTORIES

The path labelled B in Figure 2 has an exo-atmospheric segment which satisfies the altitude ceiling. The nature of this segment is completely determined by the dynamic state of the vehicle as it leaves the atmosphere. The derivation of the state at any point of the Kepler ellipse as explicit functions of the radius and velocity vectors at the edge of the atmosphere is given in Appendix A. The solution is evaluated, in particular, for the state at the point of maximum altitude and the re-entry point. These solutions are converted to the spherical coordinate system used here in Appendix B.

Energy, E,* and angular momentum, h, are conserved in the two body problem. The return trajectory has negative energy and this fact is used to isolate the escape trajectories. Thus:

$$E = u_1^2 + v_1^2 + (w_1 + \Omega_e r_1 \sin \theta_1)^2 - \frac{2\mu_e}{r_1} < 0$$

Where the subscripts 1 refer to the values of the velocity and position components at the edge of the atmosphere. In particular, $r_1 = r_A$. The time T_1 is determined when $r = r_A$, the second time, and at this time E is evaluated. If it is negative, we can evaluate the maximum altitude from the expression:

$$r_2 = \frac{\mu_e + \sqrt{\mu_e^2 + h^2 E}}{-E}$$

Where

$$h^2 = r_1^2 \left[v_1^2 + (w_1 + \Omega_e r_1 \sin \theta_1)^2 \right] .$$

This condition can be used to separate the return trajectories which satisfy the altitude constraint from those which violate it. Thus:

$$r_2 < r_{max}$$

distinguishes satisfactory skip trajectories.

*E, as used here, is equal to energy divided by m/2.

The non-linear differential equations of motion are integrated numerically from t_o to T_1, but this is unnecessary for the time interval from T_1 to T_3. Section 6 lists the solutions for the states at the top of the trajectory and the re-entry point as functions of the state at T_1. At T_1 these calculations are performed and the results printed. At T_3 the numerical integration is resumed using the values of the state at T_3 as "initial" conditions.

The adjoint differential equations are integrated backward from T to t_o. Again it is not necessary to integrate numerically over the skip portion of the trajectory. The derivation for the expressions which relate the values of the influence functions at T_1 to those at T_3 is given in Appendix C. The solutions are listed in Section 6. Suspension of the numerical integration for the time interval from T_3 to T_1 for all the influence functions represents a considerable saving in computer time.

This modification of the steepest-ascent procedure as well as those discussed in sections 5.3 and 5.4 are shown in Figure 4, Steepest-Ascent Optimization Procedure, Flow Chart B.

5.3 UNSATISFACTORY SKIP TRAJECTORIES

Re-entry trajectories like the one labelled C in Figure 2 violate the altitude ceiling. That this will happen is known at T_1 as soon as r_2 is calculated from the expression:

$$r_2 = \frac{\mu_e + \sqrt{\mu_e^2 + h^2 E}}{-E}$$

with $E < 0$. The altitude constraint requires that

$$\frac{\mu_e + \sqrt{\mu_e^2 + h^2 E}}{-E} < r_{max}$$

This condition can be included in the steepest-ascent procedure by using an intermediate point constraint. Its contribution to the calculation of the change in the control functions is treated in the same way as that of a terminal constraint except its influence function is computed over the time interval $[t_o, T_1]$ instead of $[t_o, T]$.

The intermediate point constraint is then:

$$\Psi^I = \frac{\mu_e + \sqrt{\mu_e^2 + h^2 E}}{-E} - r_{max} < 0$$

with stopping condition :

$$\Psi_p^I = r - r_A \text{ , second time}^* = 0$$

The influence function, $\underline{\lambda}_{\Psi^I}(t)$ then has "initial" value:

$$\underline{\lambda}_{\Psi^I}(T_1) = \frac{\partial \Psi^I}{\partial \underline{x}}(T_1) - \frac{\dot{\Psi}^I(T_1)}{\dot{r}(T_1)} \frac{\partial r}{\partial \underline{x}}(T_1)$$

Where

$$\frac{\partial \Psi^I}{\partial \underline{x}}(T_1) \equiv \left[\frac{\partial \Psi^I}{\partial u}, \frac{\partial \Psi^I}{\partial v}, \frac{\partial \Psi^I}{\partial w}, \frac{\partial \Psi^I}{\partial r}, \frac{\partial \Psi^I}{\partial \theta}, \frac{\partial \Psi^I}{\partial \phi} \right]' \Bigg|_{T_1}$$

$$\frac{\partial r}{\partial \underline{x}}(T_1) = \left[0, 0, 0, 1, 0, 0 \right]' .$$

The adjoint differential equations are then integrated from T_1 to t_o using $\underline{\lambda}_{\Psi^I}(T_1)$ to give the influence function for the intermediate point constraint, $\underline{\lambda}_{\Psi^I}(t)$ defined over $\left[t_o, T_1 \right]$.

In the expression for the change in the control variable program $\underline{\delta\alpha}(t)$ given in equation (18), the matrix of influence coefficients associated with the terminal constraints Λ_Ψ must be augmented by $\underline{\lambda}_{\Psi^I}$ during the time interval $[t_o, T_1]$. This is true also for Λ_Ψ occurring in the integrals in equation (19). This addition is shown in Figure 4, Steepest-Ascent Optimization Procedure, Flow Chart B.

*I.e., $r = r_A$ the second time after initial entry from $r(0) > r_a$, or more generally stated, Ψ_p^I determined by $r - r_A = 0$ and $\dot{r}$ positive.

5.4 ESCAPE TRAJECTORIES

A re-entry vehicle which penetrates the atmosphere and leaves it again with non-negative energy is on an escape trajectory. It may be possible to alter its control program sufficiently so that the trajectory is converted into a return one. The steepest-ascent procedure is precisely the tool to do this job. As shown in Figure 4, when the energy is computed at the edge of the atmosphere and found to be non-negative, the original problem is bypassed and the desired pay-off and terminal constraints replaced by $\Phi = -E$, i.e. energy to be minimized and only one terminal constraint, the stopping condition, $\Psi_p = r - r_A$, second time = 0 or $T = T_1^*$. Thus the control program over the time interval $[t_o, T_1]$ is altered iteratively until the energy at T_1 becomes negative or until it has been minimized. In the first case, we have succeeded in correcting the control program sufficiently so that the escape trajectory has been converted into a return one and the original problem is resumed. In the second case, we have minimized the energy at T_1, but it is still positive or zero. This will happen for high speed, shallow re-entries where the vehicle's negative lifting capability is insufficient to keep the vehicle in the atmosphere long enough to dissipate enough of its energy. The altitude constraint cannot be satisfied and the problem is ill-defined.

* If penalty functions are being used to achieve in-flight inequality constraints on acceleration or heating rate, they should be constrained to appropriate terminal values during this minimization.

STEEPEST-ASCENT OPTIMIZATION PROCEDURE
FLOW CHART B

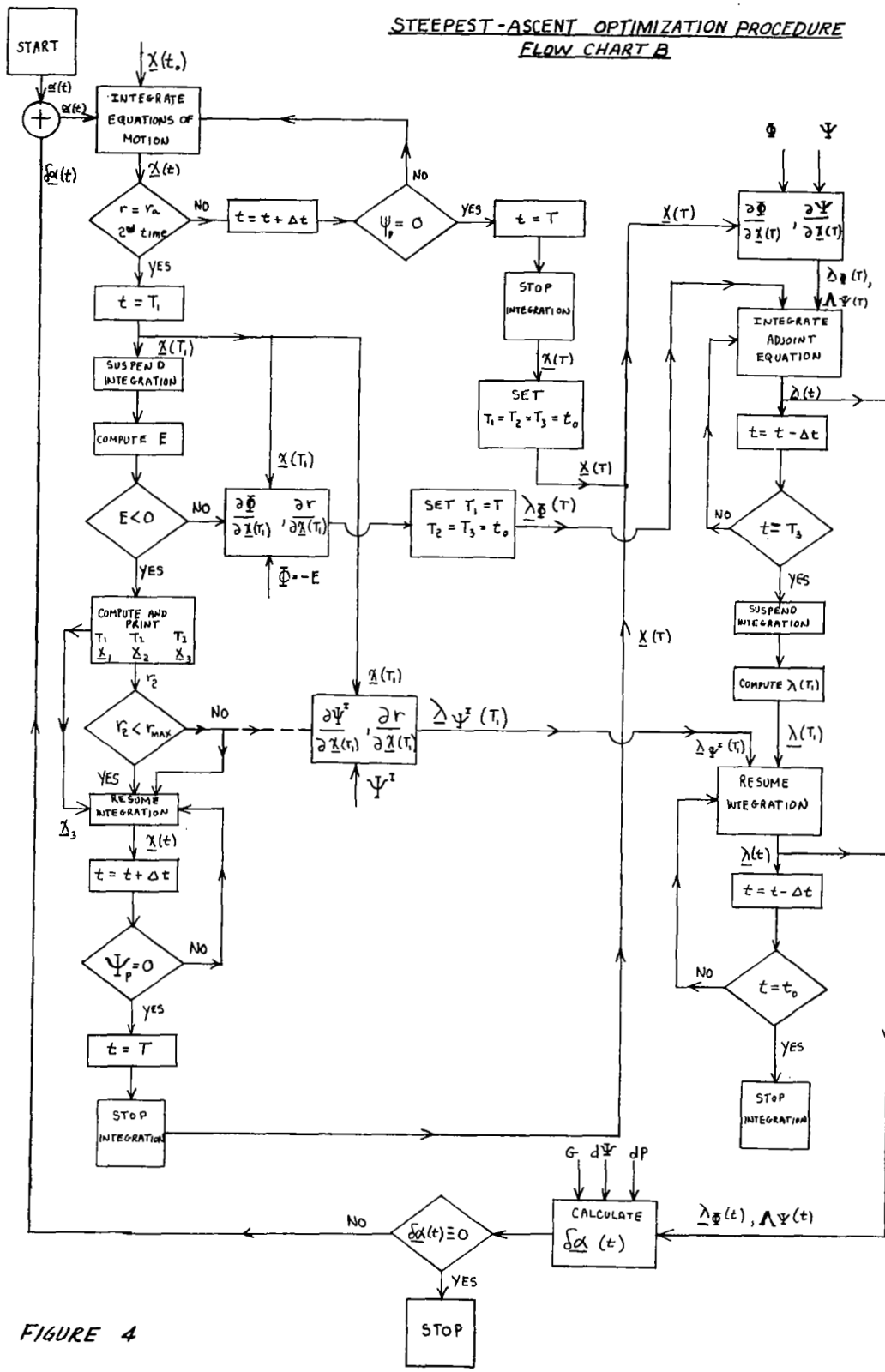

FIGURE 4

6. ANALYTIC SOLUTIONS FOR EXO-ATMOSPHERIC SEGMENTS OF PATHS

A typical re-entry altitude vs time history which includes one exo-atmospheric segment that is a Keplerian ellipse is shown in Figure 5.

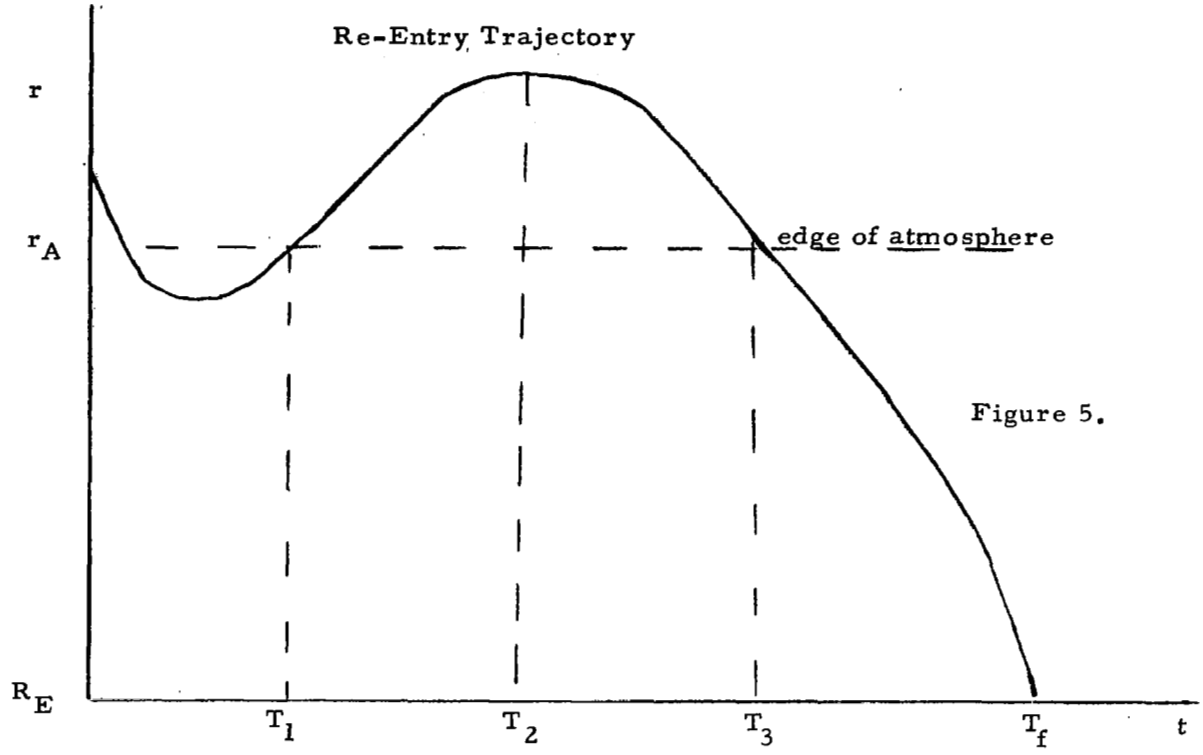

Figure 5.

The times T_1, T_2 and T_3 are the time the vehicle exits the atmosphere, the time of maximum altitude and the re-entry time respectively. The dynamic states at T_2 and T_3 are determined by the dynamic state at T_1 for an inverse square gravitational field. The solutions are derived in Appendix A. These solutions are converted to the spherical coordinate system shown in Appendix B.

When the differential equations of motion can be integrated analytically from T_1 to T_3, the adjoint equations can also be integrated analytically from T_3 to T_1. The proof of this is given in Appendix C. If the analytic solution for the j^{th} state variable is:

$$x_j(T_3) = g_j\left[x_1(T_1), x_2(T_1), \ldots, x_n(T_1)\right] \text{ for } j = 1, 2, \ldots n.$$

then:

$$\lambda_j (T_1) = \sum_{i=1}^{n} \lambda_i (T_3) \frac{\partial g_i}{\partial x_j (T_1)} \quad \text{for } j = 1, 2, \ldots, n.$$

This relation, together with the solutions g_i listed below yield $\underline{\lambda}(T_1)$ in terms of $\underline{\lambda}(T_3)$. This applies to all the influence functions $\underline{\lambda}_\Phi$ and Λ_Ψ.

The results are listed here.

For

$$E = u_1^2 + v_1^2 + (w_1 + \Omega_e r_1 \sin \theta_1)^2 - \frac{2\mu_e}{r_1}$$

$$h^2 = r_1^2 \left[v_1^2 + (w_1 + \Omega_e r_1 \sin \theta_1)^2 \right]$$

$$e = \sqrt{1 + \frac{h^2 E}{\mu_e^2}}$$

where the dynamic state at T_1 is denoted by $(r_1, \theta_1, \phi_1, u_1, v_1, w_1)$, Ω_e is the constant earth rotation rate and μ_e is the gravitational constant. The states at T_2 and T_3 are given by:

$$r_2 = \frac{h^2}{\mu_e (1-e)} = \frac{-\mu_e - \sqrt{\mu_e^2 + h^2 E}}{E}$$

$$\theta_2 = \cos^{-1} \left[\frac{1}{e} \left(1 - \frac{h^2}{r_1 \mu_e} \right) \cos \theta_1 - \frac{u_1 r_1 v_1}{\mu_e e} \sin \theta_1 \right]$$

$$\sin \theta_2 = \sqrt{1 - \cos \theta_2}$$

since $0 \leq \theta_2 \leq \pi$.

$$\phi_2 = \phi_1 + \Omega_e (T_1 - T_2)$$
$$+ \tan^{-1} \left\{ \frac{w_1 + \Omega_e r_1 \sin \theta_1}{\frac{\mu_e}{u_1 r_1} \left(1 - \frac{h^2}{r_1 \mu_e} \right) \sin \theta_1 + v_1 \cos \theta_1} \right\}$$

$$u_2 = 0$$

$$v_2 = \frac{e - 1}{e \sin \theta_2} \left\{ v_1 \left(1 - \frac{\mu_e r_1}{h^2} \right) \sin \theta_1 - u_1 \cos \theta_1 \right\}$$

$$w_2 = w_1 \frac{r_1}{r_2} \frac{\sin \theta_1}{\sin \theta_2} + \Omega_e \frac{r_1^2 \sin^2 \theta_1 - r_2^2 \sin^2 \theta_2}{r_2 \sin \theta_2}$$

$$T_2 = T_1 + \frac{h^2 u_1 r_1}{\mu_e^2 (1 - e^2)}$$
$$+ \frac{2 h^3}{\mu_e^2 (1 - e^2)^{3/2}} \left[\frac{\pi}{2} - \tan^{-1} \left(\frac{u_1 r_1 r_2}{h (r_2 - r_1)} \sqrt{\frac{1 - e}{1 + e}} \right) \right]$$

$$r_3 = r_1$$

$$\theta_3 = \cos^{-1}\left[\left(1 - 2\frac{u_1^2 h^2}{e^2 \mu_e^2}\right)\cos\theta_1 - \frac{2 r_1 u_1 v_1}{e^2 \mu_e}\left(1 - \frac{h^2}{\mu_e r_1}\right)\sin\theta_1\right]$$

$$\sin\theta_3 = \sqrt{1 - \cos^2\theta_3}$$

for $0 \leq \theta_3 \leq \pi$

$$\phi_3 = \phi_1 + \Omega_e (T_1 - T_3) + \tan^{-1}\left\{\frac{2 u_1 (\mu_e r_1 - h^2)(w_1 + \Omega_e r_1 \sin\theta_1)}{(e^2 \mu_e^2 - 2 u_1^2 h^2)\sin\theta_1 + 2 u_1 v_1 (\mu_e r_1 - h^2)\cos\theta_1}\right\}$$

$$u_3 = -u_1$$

$$v_3 = \frac{1}{e^2 \sin\theta_3}\left\{-2 u_1 \cos\theta_1\left[\frac{u_1^2 h^2}{\mu_e^2} + \left(\frac{h^2}{\mu_e r_1} - 1\right)\right] + v_1 \sin\theta_1\left[e^2 + \frac{2 u_1^2 h^2}{\mu_e^2} - \frac{4 u_1^2 r_1}{\mu_e}\right]\right\}$$

$$w_3 = w_1 \frac{\sin\theta_1}{\sin\theta_3} + \Omega_e r_1 \frac{\sin^2\theta_1 - \sin^2\theta_3}{\sin\theta_3} .$$

$$T_3 = 2 T_2 - T_1$$

$$\lambda_u(TI) = \frac{\partial \Theta_3}{\partial u_1} \lambda_\Theta(T_3) + \frac{\partial \phi_3}{\partial u_1} \lambda_\phi(T_3) + \lambda_u(T_3) + \frac{\partial v_3}{\partial u_1} \lambda_v(T_3) + \frac{\partial w_3}{\partial u_1} \lambda_w(T_3)$$

$$\lambda_v(TI) = \frac{\partial \Theta_3}{\partial v_1} \lambda_\Theta(T_3) + \frac{\partial \phi_3}{\partial v_1} \lambda\phi(T_3) + \frac{\partial v_3}{\partial v_1} \lambda_v(T_3) + \frac{\partial w_3}{\partial v_1} \lambda_w(T_3)$$

$$\lambda_w(TI) = \frac{\partial \Theta_3}{\partial w_1} \lambda_\Theta(T_3) + \frac{\partial \phi_3}{\partial w_1} \lambda_\phi(T_3) + \frac{\partial v_3}{\partial w_1} \lambda_v(T_3) + \frac{\partial w_3}{\partial w_1} \lambda_w(T_3)$$

$$\lambda_r(TI) = \lambda_r(T_3) + \frac{\partial \Theta_3}{\partial r_1} \lambda_\Theta(T_3) + \frac{\partial \phi_3}{\partial r_1} \lambda_\phi(T_3) + \frac{\partial v_3}{\partial r_1} \lambda_v(T_3) + \frac{\partial w_3}{\partial r_1} \lambda_w(T_3)$$

$$\lambda_\Theta(TI) = \frac{\partial \Theta_3}{\partial \Theta_1} \lambda_\Theta(T_3) + \frac{\partial \phi_3}{\partial \Theta_1} \lambda_\phi(T_3) + \frac{\partial v_3}{\partial \Theta_1} \lambda_v(T_3) + \frac{\partial w_3}{\partial \Theta_1} \lambda_w(T_3)$$

$$\lambda_\phi(TI) = \lambda_\phi(T_3)$$

7. CONCLUSIONS AND RECOMMENDATIONS

Recent developments at Raytheon, in the mathematical theory of the steepest-ascent technique have produced a new, direct method for incorporating in-flight inequality constraints into the optimization procedure. Originally, the steepest-ascent method could handle terminal constraints only. The penalty function concept was an ingeneous way of converting in-flight inequality constraints into terminal constraints. Computer programs for production use were written making wide use of penalty functions and were extremely effective tools for many trajectory optimization studies.

Research was conducted to extend the capability of the steepest-ascent technique, especially in the area of in-flight inequality constraints. A direct method was found which produced optimal trajectories with segments which lie on the constraint boundary. The necessary conditions for an extremum had to be extended to provide optimal switching conditions. Test computer programs were written so that a comparison with the penalty function method could be made. The results proved that the direct method was much faster in finding the optimal trajectory. This study is described in Reference 3.

The re-entry corridor study described in the first part of this report included a maximum altitude constraint. The penalty function method had proved adequate for satisfying altitude ceilings within the sensible atmosphere; however, the optimal trajectories required for this study were subject to exo-atmospheric altitude ceilings. The penalty function method did not provide sufficient control for sensitive high-speed trajectories.

The direct method of Reference 3 had been used to find optimal, high-speed re-entry trajectories subject to altitude ceilings within the sensible atmosphere. In the current study, attention was directed to extend the direct method to solve problems with exo-atmospheric altitude ceilings. It became clear that such problems could be solved using an intermediate point constraint which acts directly to constrain the maximum altitude. This method is particularly attractive for use with a spherical earth. In the inverse-square gravitational field, an analytic expression can be found which relates the maximum altitude to the dynamic state with which the vehicle leaves the atmosphere. For such a

situation, the intermediate point constraint can be placed on a function of the state at the edge of the atmosphere. Thus the optimization process may be employed with great effectiveness during the interval when the vehicle initially re-enters the atmosphere to satisfy an exo-atmospheric altitude ceiling which is reached much later in the trajectory. Maximum altitude constraints, whether the specified ceilings are inside or outside the atmosphere, now can be handled by the direct method.

On the basis of work initiated during the concluding months of the current contract, it appears that if the mathematical model for the optimization problem uses an oblate earth, the intermediate point constraint must be set directly to maximum altitude and applied at that point. It would be useful if the effect of earth oblateness on the Keplerian trajectory could be expressed analytically. Then it would be possible to apply the intermediate point constraint on a function of the dynamic state of the vehicle at the edge of the atmosphere for either spherical or oblate earth. In addition, numerical integration could be suspended over the skip-out portion of the trajectory for an oblate earth also, and considerable saving in computer time would result. Although the current work in the development of the necessary analytical relations has proved unfruitful, it is highly recommended that further effort be expended in this area because of the high probability that future trajectory studies, involving extremely high entry velocities, will include many exo-atmospheric segments.

REFERENCES

1. Bryson, A. E., and Denham, W. F., A Steepest-Ascent Method for Solving Optimum Programming Problems, Trans. of ASME, Series E: Journal of Applied Mechanics, Vol. 29, No. 2, June 1962, pp 247-257; also Raytheon Company, Report BR-1303, Aug. 10, 1961.

2. Bryson, A. E.; Denham, W. F.; Dreyfus, S. E.; Optimal Programming Problems with Inequality Constraints I: Necessary Conditions for External Solutions. AIAA Journal, November 1963.

3. Denham, W. F. and Bryson, A. E., Optimal Programming Problems with Inequality Constraints II: Solution by Steepest-Ascent. AIAA Journal, January 1964.

APPENDIX A

KEPLERIAN TRAJECTORIES

Given:
$$\ddot{\underline{r}} = -\frac{\mu_e}{r^3}\,\underline{r} \tag{A1}$$

$$\underline{r}(t_o) \equiv \underline{r}_o \text{ and } \dot{\underline{r}}(t_o) \equiv \underline{v}_o \tag{A2}$$

To Find: $\underline{r}(t)$ and $\dot{\underline{r}}(t)$

I. Constants of the Integration

Evaluating the derivative and using (A1), we have:

$$\frac{d}{dt}(\underline{r} \times \dot{\underline{r}}) = \underline{r} \times \ddot{\underline{r}} + \dot{\underline{r}} \times \dot{\underline{r}}$$

$$= \underline{r} \times \left[-\frac{\mu_e}{r^3}\,\underline{r} \right] + 0$$

$$= 0 .$$

Thus:

$$\underline{r} \times \dot{\underline{r}} = \text{constant} \equiv \underline{h} \tag{A3}$$

In Particular:

$$\underline{h} = \underline{r}_o \times \underline{v}_o \tag{A4}$$

Equation (A3) shows the path is planar. Choose the (ξ, η) plane to be the plane of $\underline{r}_o$ and $\underline{v}_o$, assuming these vectors are not collinear. The ζ axis is perpendicular to this plane and in the direction of $\underline{h}$.

Evaluating the derivative,

$$\frac{d}{dt}(\dot{\underline{r}} \times \underline{h}) = \ddot{\underline{r}} \times \underline{h} + \dot{\underline{r}} \times \dot{\underline{h}}$$

using (A1) and (A3) and expanding the vector triple product, we have:

$$\frac{d}{dt}(\dot{\underline{r}} \times \underline{h}) = -\frac{\mu_e}{r^3} \underline{r} \times (\underline{r} \times \dot{\underline{r}}) + 0$$

$$= -\frac{\mu_e}{r^3} \left[(\underline{r} \cdot \dot{\underline{r}}) \underline{r} - (\underline{r} \cdot \underline{r}) \dot{\underline{r}} \right]$$

$$= \mu_e \left[\underline{r} \frac{d}{dt} (\frac{1}{r}) + (\frac{1}{r}) \dot{\underline{r}} \right]$$

$$= \frac{d}{dt} (\frac{\mu_e}{r} \underline{r})$$

Thus:

$$\dot{\underline{r}} \times \underline{h} = \frac{\mu_e}{r} \underline{r} + \text{constant} \tag{A5}$$

We define the vector constant of integration to be $\mu_e \underline{e}$ where

$$\underline{e} \equiv \frac{1}{\mu_e} \dot{\underline{r}} \times \underline{h} - \frac{1}{r} \underline{r} \tag{A6}$$

In particular:

$$\underline{e} = \frac{1}{\mu_e} \underline{v}_o \times \underline{h} - \frac{1}{r_o} \underline{r}_o \tag{A7}$$

Using (A4):

$$\underline{e} = \frac{1}{\mu_e} \underline{v}_o \times (\underline{r}_o \times \underline{v}_o) - \frac{1}{r_o} \underline{r}_o \tag{A8}$$

Expanding the triple product:

$$\underline{e} = \left[\frac{(\underline{v}_o \cdot \underline{v}_o)}{\mu_e} - \frac{1}{r_o}\right] \underline{r}_o - \frac{1}{\mu_e} (\underline{v}_o \cdot \underline{r}_o)\, \underline{v}_o \qquad \text{(A9)}$$

Note that $\underline{e}$ is in the (ξ, η) plane. Choose the ξ axis in the $\underline{e}$ direction and since the ζ axis has been chosen in the $\underline{h}$ direction, the η axis completes the right hand triad. The coordinate system is then:

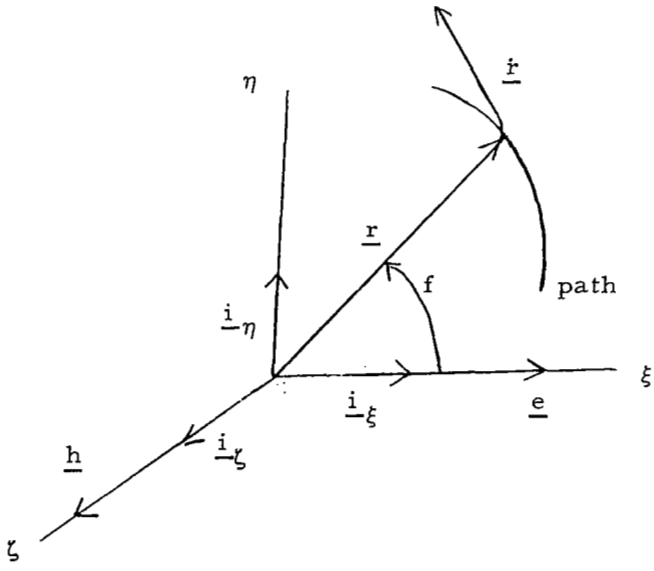

with $\underline{i}_\xi$, $\underline{i}_\eta$, $\underline{i}_\zeta$ unit vectors.

II. Solution in terms of Initial State

From the preceding sketch, we see:

$$\underline{r} = \underline{i}_\xi \, r \cos f + \underline{i}_\eta \, r \sin f \tag{A10}$$

Differentiating, we have:

$$\begin{aligned} \dot{\underline{r}} = \underline{i}_\xi \left[\frac{dr}{dt} \cos f - r \frac{df}{dt} \sin f \right] \\ + \underline{i}_\eta \left[\frac{dr}{dt} \sin f + r \frac{df}{dt} \cos f \right] \end{aligned} \tag{A11}$$

We need expressions for r, $\frac{dr}{dt}$, $\frac{df}{dt}$ in terms of the independent variable f and fn $\underline{i}_\xi$ and $\underline{i}_\eta$ in terms of $\underline{r}_o$ and $\underline{v}_o$. (A6) can be written:

$$\frac{1}{r} \underline{r} = \frac{1}{\mu_e} \dot{\underline{r}} \times \underline{h} - \underline{e}$$

Multiplying by $\underline{r}$, we have:

$$r = \frac{1}{\mu_e} (\dot{\underline{r}} \times \underline{h}) \cdot \underline{r} - \underline{e} \cdot \underline{r}$$

$$= \frac{1}{\mu_e} (\underline{r} \times \dot{\underline{r}}) \cdot \underline{h} - \underline{e} \cdot \underline{r}$$

$$= \frac{h^2}{\mu_e} - er \cos f$$

Thus:

$$r = \frac{\frac{h^2}{\mu_e}}{1 + e \cos f} \tag{A12}$$

which describes the path.

Recalling (A3):

$$\underline{h} = \underline{r} \times \dot{\underline{r}}$$

and resolving $\dot{\underline{r}}$ into radial and transverse components, we have:

$$h = r^2 \frac{df}{dt} \tag{A13}$$

Differentiating (A12) and using (A13), we get:

$$\frac{dr}{dt} = \frac{e\,\mu_e}{h} \sin f \tag{A14}$$

(A9) can be written as:

$$e\,\underline{i}_\xi = \left[\frac{(\underline{v}_o \cdot \underline{v}_o)}{\mu_e} - \frac{1}{r_o}\right] \underline{r}_o - \frac{1}{\mu_e} (\underline{v}_o \cdot \underline{r}_o)\, \underline{v}_o$$

Thus: $$\underline{i}_\xi = \frac{1}{e\mu_e}\left[(\underline{v}_o \cdot \underline{v}_o - \frac{\mu_e}{r_o})\, \underline{r}_o - (\underline{v}_o \cdot \underline{r}_o)\, \underline{v}_o \right] \tag{A15}$$

But

$$\underline{h} = h\, \underline{i}_\zeta$$

And

$$\underline{i}_\eta = \underline{i}_\zeta \times \underline{i}_\xi$$

Thus:

$$\underline{i}_\eta = \frac{1}{e\mu_e h}\left[(\underline{v}_o \cdot \underline{v}_o - \frac{\mu_e}{r_o})\, (\underline{h} \times \underline{r}_o) - (\underline{v}_o \cdot r_o)\, (\underline{h} \times \underline{v}_o) \right]$$

or

$$\underline{i}_\eta = \frac{1}{eh}\left[\frac{(\underline{v}_o \cdot \underline{r}_o)}{r_o}\, \underline{r}_o + (\frac{h^2}{\mu_e} - r_o)\, \underline{v}_o \right] \tag{A16}$$

Substituting (A12), (A13), (A14), (A15) and (A16) into (A10) and (A11), we have:

$$\underline{r} = \frac{\frac{h^2}{e\,\mu_e}}{1 + e\cos f} \left\{ \left[\left(\frac{\underline{v}_o \cdot \underline{v}_o}{\mu_e} - \frac{1}{r_o} \right) \cos f + \frac{(\underline{v}_o \cdot \underline{r}_o)}{h\, r_o} \sin f \right] \underline{r}_o \right.$$

$$\left. + \left[- \frac{(\underline{v}_o \cdot \underline{r}_o)}{\mu_e} \cos f + \left(\frac{h}{\mu_e} - \frac{r_o}{h} \right) \sin f \right] \underline{v}_o \right\} \quad \text{(A17)}$$

$$\dot{\underline{r}} = \frac{\mu_e}{h^c} \left\{ \left[- \left(\frac{\underline{v}_o \cdot \underline{v}_o}{\mu_e} - \frac{1}{r_o} \right) \sin f + \frac{(\underline{v}_o \cdot \underline{r}_o)}{h\, r_o} (e + \cos f) \right] \underline{r}_o \right.$$

$$\left. + \left[\frac{(\underline{v}_o \cdot \underline{r}_o)}{\mu_e} \sin f + \left(\frac{h}{\mu_e} - \frac{r_o}{h} \right) (e + \cos f) \right] \underline{v}_o \right\} \quad \text{(A18)}$$

With

$$h = \left| \underline{r}_o \times \underline{v}_o \right| \quad \text{(A19)}$$

And

$$e = \sqrt{1 + \frac{h^2}{\mu_e} \left(\frac{\underline{v}_o \cdot \underline{v}_o}{\mu_e} - \frac{2}{r_o} \right)} \quad \text{(A20)}$$

III. Special Cases for Elliptical Trajectories

A. The maximum value of r occurs for $f = \pi$.

$$\underline{r}(\pi) = \frac{1}{e}\left(\frac{h^2}{1-e}\right)\left[\left(\frac{1}{r_o\mu_e} - \frac{\underline{v}_o \cdot \underline{v}_o}{\mu_e^2}\right)\underline{r}_o + \frac{(\underline{v}_o \cdot \underline{r}_o)}{\mu_e^2}\underline{v}_o\right] \tag{A21}$$

$$\dot{\underline{r}}(\pi) = \frac{1}{e}\left(\frac{1-e}{h^2}\right)\left[-\frac{\mu_e}{r_o}(\underline{v}_o \cdot \underline{r}_o)\underline{r}_o + (r_o\mu_e - h^2)\underline{v}_o\right] \tag{A22}$$

B. Re-entry occurs for $f = 2\pi - f_o$.

$$\underline{r}(2\pi - f_o) = \left[1 - \frac{2(\underline{v}_o \cdot \underline{r}_o)^2}{r_o\mu_e e^2}\right]\underline{r}_o + \frac{2(\underline{v}_o \cdot \underline{r}_o)}{\mu_e^2 e^2}\left(r_o\mu_e - h^2\right)\underline{v}_o \tag{A23}$$

$$\dot{\underline{r}}(2\pi - f_o) = \frac{2(\underline{v}_o \cdot \underline{r}_o)}{r_o e^2}\left(\frac{\underline{v}_o \cdot \underline{v}_o}{\mu_e} - \frac{1}{r_o}\right)\underline{r}_o + \left[1 - \frac{2(\underline{v}_o \cdot \underline{r}_o)^2}{r_o\mu_e e^2}\right]\underline{v}_o \tag{A24}$$

IV. Time Dependence

The last integration proceeds from equations (A13) and (A12).

$$\frac{df}{(1 + e \cos f)^2} = \frac{\mu_e^2 \, dt}{h^3}$$

To integrate this, let

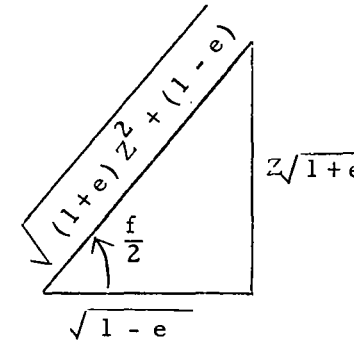

$$\tan \frac{f}{2} \equiv \frac{\sqrt{1+e}}{\sqrt{1-e}} \, Z$$

$$\frac{df}{2} \sec^2 \frac{f}{2} = \frac{\sqrt{1+e}}{\sqrt{1-e}} \, dZ$$

$$\cos f = \cos^2 \frac{f}{2} - \sin^2 \frac{f}{2}$$

$$\cos f = \frac{(1-e) - (1+e) Z^2}{(1-e) + (1+e) Z^2}$$

This substitution yields:

$$\frac{2 \, dZ \left[Z^2 + \frac{1-e}{1+e} \right]}{(1-e)\sqrt{1-e^2} \, (1+Z^2)^2} = \frac{\mu_e^2 \, dt}{h^3}$$

Integration gives:

$$\frac{2}{(1-e^2)^{3/2}} \left[\tan^{-1} Z - \frac{e Z}{1+Z^2} \right] \Bigg|_{Z_o}^{Z} = \frac{\mu_e^2}{h^3} (t - t_o)$$

Returning to the independent variable f , we have:

$$\frac{2}{(1-e^2)^{3/2}}\left[\tan^{-1}\sqrt{\frac{1-e}{1+e}}\,\tan\frac{f}{2}-\frac{e\sqrt{1-e^2}\sin f}{2(1+e\cos f)}\right]\Bigg|_{f_o}^{f}=\frac{\mu_e^2}{h^3}(t-t_o)$$

This becomes:

$$t=t_o+\frac{2h^3}{\mu_e^2(1-e^2)^{3/2}}\left[\tan^{-1}\sqrt{\frac{1-e}{1+e}}\,\tan\frac{f}{2}-\tan^{-1}\sqrt{\frac{1-e}{1+e}}\,\tan\frac{f_o}{2}\right]$$

$$-\frac{eh^3}{\mu_e^2(1-e^2)}\left[\frac{\sin f}{1+e\cos f}-\frac{\sin f_o}{1+e\cos f_o}\right]. \qquad \text{(A25)}$$

$$f_o \le f \le \pi$$

For the special cases discussed in Section III, we have:

A. $f = \pi$

$$t(\pi)=t_o+\frac{2h^3}{\mu_e^2(1-e^2)^{3/2}}\left[\frac{\pi}{2}-\tan^{-1}\frac{\sqrt{1-e}\,(\underline{v}_o\cdot\underline{r}_o)\,h}{\sqrt{1+e}\left[h^2+\mu_e r_o(e-1)\right]}\right]$$

$$+\frac{h^2(\underline{v}_o\cdot\underline{r}_o)}{\mu_e^2(1-e^2)}. \qquad \text{(A26)}$$

B. $f = 2\pi - f_o$

$$t(2\pi-f_o)=2t(\pi)-t_o \qquad \text{(A27)}$$

Reference: Battin, Richard H., Astronautical Guidance, McGraw-Hill, New York, 1964 p. 15-21.

APPENDIX B

COORDINATE TRANSFORMATION

The results of Appendix A are in a fixed rectangular coordinate system. The equations of motion are in a constantly rotating spherical coordinate system. This appendix will establish the transformation.

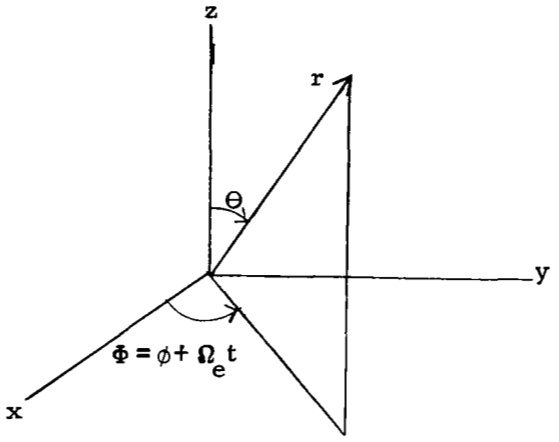

We have:

$$\begin{aligned} x &= r \sin\theta \cos\Phi \\ y &= r \sin\theta \sin\Phi \\ z &= r \cos\theta \end{aligned} \tag{B 1}$$

Using the definitions:

$$\begin{aligned} \dot{r} &= u \\ \dot{\theta} &= \frac{v}{r} \\ \dot{\phi} &= \frac{w}{r \sin\theta} \end{aligned} \tag{B 2}$$

and differentiating equations (B 1) we get:

$$\begin{aligned} \dot{x} &= (u \sin\theta + v \cos\theta) \cos\Phi - r\dot{\Phi} \sin\theta \sin\Phi \\ \dot{y} &= (u \sin\theta + v \cos\theta) \sin\Phi + r\dot{\Phi} \sin\theta \cos\Phi \\ \dot{z} &= u \cos\theta - v \sin\theta \end{aligned} \tag{B 3}$$

Inverting (B1) and (B3) we have:

$$r = \sqrt{x^2 + y^2 + z^2} \tag{B4}$$

$$\Theta = \cos^{-1} \frac{z}{r} \tag{B5}$$

$$\Phi = \tan^{-1} \frac{y}{x} \tag{B6}$$

$$u = \frac{x\dot{x} + y\dot{y} + z\dot{z}}{r} \tag{B7}$$

$$v = \frac{uz - r\dot{z}}{\sqrt{x^2 + y^2}} \tag{B8}$$

$$\dot{\Phi} = \frac{x\dot{y} - y\dot{x}}{x^2 + y^2} \tag{B9}$$

Note also:

$$\dot{x}^2 + \dot{y}^2 + \dot{z}^2 = u^2 + v^2 + r^2\dot{\Phi}^2 \sin^2 \Theta \tag{B10}$$

But Appendix A in equations (A11) and (A12) yields:

$$\begin{bmatrix} x \\ y \\ z \end{bmatrix} = C_1(f) \begin{bmatrix} x_o \\ y_o \\ z_o \end{bmatrix} + C_2(f) \begin{bmatrix} \dot{x}_o \\ \dot{y}_o \\ \dot{z}_o \end{bmatrix} \tag{B11}$$

$$\begin{bmatrix} \dot{x} \\ \dot{y} \\ \dot{z} \end{bmatrix} = C_3(f) \begin{bmatrix} x_o \\ y_o \\ z_o \end{bmatrix} + C_4(f) \begin{bmatrix} \dot{x}_o \\ \dot{y}_o \\ \dot{z}_o \end{bmatrix} \tag{B12}$$

where C_1, C_2, C_3, and C_4 are functions of f and the initial conditions.

Using (B11) and (B4) we have:

$$r = \sqrt{(C_1 x_o + C_2 \dot{x}_o)^2 + (C_1 y_o + C_2 \dot{y}_o)^2 + (C_1 z_o + C_2 \dot{z}_o)^2}$$

or

$$r = \sqrt{C_1^2 r_o^2 + 2C_1 C_2 r_o u_o + C_2^2 \left[u_o^2 + v_o^2 + r_o^2 \dot{\Phi}_o^2 \sin^2 \Theta_o\right]} \qquad \text{(B13)}$$

or

$$r = \sqrt{(C_1 r_o + C_2 u_o)^2 + C_2^2 \left[v_o^2 + r_o^2 \dot{\Phi}_o^2 \sin^2 \Theta_o\right]} \qquad \text{(B14)}$$

Using (B5) and (B11) we have:

$$\Theta = \cos^{-1} \frac{C_1 z_o + C_2 \dot{z}_o}{r}$$

$$\Theta = \cos^{-1} \frac{\left(C_1 r_o + C_2 u_o\right) \cos \Theta_o - C_2 v_o \sin \Theta_o}{r} \qquad \text{(B15)}$$

Using (B6) and (B11) we have:

$$\Phi = \tan^{-1} \frac{C_1 y_o + C_2 \dot{y}_o}{C_1 x_o + C_2 \dot{x}_o}$$

$$= \tan^{-1} \frac{\dfrac{y_o}{x_o} + \dfrac{C_2}{C_1} \dfrac{\dot{y}_o}{x_o}}{1 - \dfrac{y_o}{x_o}\left(-\dfrac{C_2}{C_1}\dfrac{\dot{x}_o}{y_o}\right)}$$

$$= \tan^{-1} \frac{\tan \Phi_o + \dfrac{C_2}{C_1}\left[\tan \Phi_o \left(\dfrac{u_o}{r_o} + \dfrac{v_o}{r_o} \cot \theta_o\right) + \dot{\Phi}_o\right]}{1 - \left[\tan \Phi_o\right]\dfrac{C_2}{C_1}\left[-\cot \Phi_o \left(\dfrac{u_o}{r_o} + \dfrac{v_o}{r_o} \cot \theta_o\right) + \dot{\Phi}_o\right]}$$

$$= \tan^{-1} \frac{\tan \Phi_o \left[1 + \dfrac{C_2}{C_1}\left(\dfrac{u_o}{r_o} + \dfrac{v_o}{r_o} \cot \theta_o\right)\right] + \dfrac{C_2}{C_1} \dot{\Phi}_o}{\left[1 + \dfrac{C_2}{C_1}\left(\dfrac{u_o}{r_o} + \dfrac{v_o}{r_o} \cot \theta_o\right)\right] - \dfrac{C_2}{C_1} \dot{\Phi}_o \tan \Phi_o}$$

$$= \tan^{-1} \frac{\tan \Phi_o + \dfrac{C_2 \dot{\Phi}_o r_o \sin \theta_o}{(C_1 \dot{r}_o + C_2 u_o) \sin \theta_o + C_2 v_o \cos \theta_o}}{1 - \tan \Phi_o \dfrac{C_2 \dot{\Phi}_o r_o \sin \theta_o}{(C_1 \dot{r}_o + C_2 u_o) \sin \theta_o + C_2 v_o \cos \theta_o}}$$

$$\Phi = \Phi_o + \tan^{-1} \frac{C_2 \dot{\Phi}_o r_o \sin \theta_o}{(C_1 \dot{r}_o + C_2 u_o) \sin \theta_o + C_2 v_o \cos \theta_o} \qquad \text{(B16)}$$

Using (B7), (B11), and (B12) we get:

$$u = \frac{(C_1x_o + C_2\dot{x}_o)(C_3x_o + C_4\dot{x}_o) + (C_1y_o + C_2\dot{y}_o)(C_3y_o + C_4\dot{y}_o)}{r}$$

$$+ \frac{(C_1z_o + C_2\dot{z}_o)(C_3z_o + C_4 + \dot{z}_o)}{r}$$

$$u = \frac{C_1C_3r_o^2 + (C_1C_4 + C_2C_3)r_ou_o + C_2C_4\left[u_o^2 + v_o^2 + r_o^2\dot{\Phi}_o^2\sin^2\Theta_o\right]}{r} \qquad \text{(B17)}$$

Using (B8), and (B11), and (B12) we have:

$$v = \frac{u\left[C_1z_o + C_2\dot{z}_o\right] - r\left[C_3z_o + C_4\dot{z}_o\right]}{r\sin\Theta}$$

$$v = \frac{\left[(C_1r_o + C_2u_o)u - (C_3r_o + C_4u_o)r\right]\cos\Theta_o - v_o\sin\Theta_o\left[C_2u - C_4r\right]}{r\sin\Theta} \qquad \text{(B18)}$$

Using (B9), (B11), and (B12) we have:

$$\dot{\Phi} = \frac{(C_1x_o + C_2\dot{x}_o)(C_3y_o + C_4\dot{y}_o) - (C_1y_o + C_2\dot{y}_o)(C_3x_o + C_4\dot{x}_o)}{r^2\sin^2\Theta}$$

$$\dot{\Phi} = \frac{(C_1C_4 - C_2C_3)\dot{\Phi}_o r_o^2\sin^2\Theta_o}{r^2\sin^2\Theta} \qquad \text{(B19)}$$

Using equations in Appendix A, the trajectory is now determined in terms of the initial state. For elliptical trajectories, let the subscript 1 denote the initial point, $f = f_1$, subscript 2, the top of the path, $f = \pi$ and subscript 3, the re-entry point, $f = 2\pi - f_1$. If the following order of computation is set up, the critical points of the trajectory may be found. All the equations necessary will be summarized here and the transformation from Φ and $\dot{\Phi}$ to ϕ and w will be included. From equations (A19) and (A20) together with the following definition of E, we have:

$$E = u_1^2 + v_1^2 + (w_1 + \Omega_e r_1 \sin \theta_1)^2 - \frac{2\mu_e}{r_1} \tag{B20}$$

$$h^2 = r_1^2 \left[v_1^2 + (w_1 + \Omega_e r_1 \sin \theta_1)^2 \right] \tag{B21}$$

$$e = \sqrt{1 + \frac{h^2 E}{\mu_e^2}} \tag{B22}$$

The terms $C_1(f), \ldots C_4(f)$ are defined in equations (B11) and (B12). For $f = \pi$, equations (A21) and (A22) show these terms to be:

$$C_1(\pi) = \frac{h^2}{e(e-1)} \left(\frac{E}{\mu_e^2} + \frac{1}{\mu_e r_1} \right) \tag{B23}$$

$$C_2(\pi) = \frac{h^2 u_1 r_1}{e(1-e)\mu_e^2} \tag{B24}$$

$$C_3(\pi) = \frac{\mu_e u_1 (e-1)}{e h^2} \tag{B25}$$

$$C_4(\pi) = \frac{e-1}{e} \left(1 - \frac{r_1 \mu_e}{h^2} \right) \tag{B26}$$

Using these last seven equations, we can now compute the state at the top of the path. Equation (A12) shows for $f = \pi$:

$$r_2 = \frac{h^2}{\mu_e (1-e)} \tag{B27}$$

An equivalent expression for this comes from equation (B14)

$$r_2 = \frac{-\mu_e - \sqrt{\mu_e^2 + h^2 E}}{E} \tag{B28}$$

Equation (B15) yields:

$$\theta_2 = \cos^{-1}\left[\frac{1}{e}\left(1 - \frac{h^2}{r_1 \mu_e}\right)\cos\theta_1 - \frac{u_1 r_1 v_1}{\mu_e e}\sin\theta_1\right] \tag{B29}$$

And

$$\sin\theta_2 = \sqrt{1 - \cos\theta_2} \tag{B30}$$

since $0 \leq \theta_2 \leq \pi$.

From equation (B16), we have:

$$\phi_2 = \phi_1 + \Omega_e (T_1 - T_2) + \tan^{-1}\left\{\frac{w_1 + \Omega_e r_1 \sin\theta_1}{\frac{\mu_e}{u_1 r_1}\left(1 - \frac{h^2}{r_1 \mu_e}\right)\sin\theta_1 + v_1 \cos\theta_1}\right\} \tag{B31}$$

At the top:

$$u_2 = 0 \tag{B32}$$

Equation (B18) gives:

$$v_2 = \frac{e-1}{e \sin \theta_2} \left\{ v_1 \left(1 - \frac{\mu_e r_1}{h^2} \right) \sin \theta_1 - u_1 \cos \theta_1 \right\} \tag{B33}$$

Equation (B19) together with the information in Figure 1 and equation (B2), yield:

$$w_2 = w_1 \frac{r_1}{r_2} \frac{\sin \theta_1}{\sin \theta_2} + \Omega_e \frac{r_1^2 \sin^2 \theta_1 - r_2^2 \sin^2 \theta_2}{r_2 \sin \theta_2} \tag{B34}$$

Equation (A26) yields:

$$T_2 = T_1 + \frac{h^2 u_1 r_1}{\mu_e^2 (1 - e^2)} + \frac{2h^3}{\mu_e^2 (1 - e^2)^{3/2}} \left[\frac{\pi}{2} - \tan^{-1} \left(\frac{u_1 r_1 r_2}{h (r_2 - r_1)} \sqrt{\frac{1-e}{1+e}} \right) \right] \tag{B35}$$

The terms $C_1(f), \ldots C_4(f)$, defined by equations (B11) and (B12), are shown to be by equations (A23) and (A24), for $f = 2\pi - f_1$:

$$C_1 (2\pi - f_1) = 1 - \frac{2 u_1^2 r_1}{\mu_e e^2} \tag{B36}$$

$$C_2 (2\pi - f_1) = \frac{2 u_1 r_1}{\mu_e^2 e^2} (r_1 \mu_e - h^2) \tag{B37}$$

$$C_3 (2\pi - f_1) = \frac{2 u_1}{e^2} \left(\frac{E}{\mu_e} + \frac{1}{r_1} \right) \tag{B38}$$

$$C_4 (2\pi - f_1) = 1 - \frac{2 u_1^2 r_1}{\mu_e e^2} \tag{B39}$$

Using these values for the C's, we can compute the state at the re-entry point from equations (B14) through (B19). Thus:

$$r_3 = r_1 \tag{B40}$$

$$\theta_3 = \cos^{-1}\left[\left(1 - 2\frac{u_1^2 h^2}{e^2 \mu_e^2}\right)\cos\theta_1 - \frac{2 r_1 u_1 v_1}{e^2 \mu_e}\left(1 - \frac{h^2}{\mu_e r_1}\right)\sin\theta_1\right] \tag{B41}$$

$$\sin\theta_3 = \sqrt{1 - \cos^2\theta_3} \tag{B42}$$

$$\text{for } 0 \leq \theta_3 \leq \pi$$

$$\phi_3 = \phi_1 + \Omega_e (T_1 - T_3) + \tan^{-1}\left\{\frac{2 u_1 (\mu_e r_1 - h^2)(w_1 + \Omega_e r_1 \sin\theta_1)}{(e^2 \mu_e^2 - 2 u_1^2 h^2)\sin\theta_1 + 2 u_1 v_1 (\mu_e r_1 - h^2)\cos\theta_1}\right\} \tag{B43}$$

$$u_3 = -u_1 \tag{B44}$$

$$v_3 = \frac{1}{e^2 \sin\theta_3}\left\{-2 u_1 \cos\theta_1\left[\frac{u_1^2 h^2}{\mu_e^2} + \left(\frac{h^2}{\mu_e r_1} - 1\right)\right] + v_1 \sin\theta_1 \left[e^2 + \frac{2 u_1^2 h^2}{\mu_e^2} - \frac{4 u_1^2 r_1}{\mu_e}\right]\right\} \tag{B45}$$

$$w_3 = w_1 \frac{\sin\theta_1}{\sin\theta_3} + \Omega_e r_1 \frac{\sin^2\theta_1 - \sin^2\theta_3}{\sin\theta_3} . \tag{B46}$$

From equation (A27), the re-entry time is

$$T_3 = 2 T_2 - T_1 \tag{B47}$$

APPENDIX C

ADJOINT EQUATIONS

If the differential equations of motion can be integrated analytically from t_o to t_f, then the adjoint equations can also be integrated analytically from t_f to t_o. The proof follows:

Given: 1. n state variables

$$x_1, x_2, \ldots, x_n \tag{C1}$$

2. n values of state variables at t_o

$$x_1^o, x_2^o, \ldots, x_n^o \tag{C2}$$

3. n differential equations

$$\dot{x}_j = f_j(x_1, x_2, \ldots, x_n), \quad j = 1, 2, \ldots, n \tag{C3}$$

4. n solutions of state variables at t_f

$$x_j^f = g_j(x_1^o, x_2^o, \ldots, x_n^o), \quad j = 1, 2, \ldots, n \tag{C4}$$

5. n adjoint variables

$$\lambda_1, \lambda_2, \ldots, \lambda_n \tag{C5}$$

6. n values of adjoint variables at t_f

$$\lambda_1^f, \lambda_2^f, \ldots, \lambda_n^f \tag{C6}$$

7. n adjoint differential equations

$$\dot{\lambda}_j = -\sum_{i=1}^{n} \frac{\partial f_i}{\partial x_j} \lambda_i, \quad j = 1, 2, \ldots, n \tag{C7}$$

To find: 1. n values of adjoint variables at t_o.

$$\lambda_1^o, \lambda_2^o, \ldots, \lambda_n^o \tag{C8}$$

Since, by (C3):

$$\dot{x}_j = f_j(x_1, x_2, \ldots, x_n) \qquad j = 1, \ldots n$$

then:

$$\delta\dot{x}_j = \sum_{i=1}^{n} \frac{\partial f_j}{\partial x_i} \delta x_i$$

and:

$$\frac{d}{dt} \delta x_j = \sum_{i=1}^{n} \frac{\partial f_j}{\partial x_i} \delta x_i \tag{C9}$$

Consider:

$$\frac{d}{dt} \left(\sum_{m=1}^{n} \lambda_m \delta x_m \right) = \sum_{m=1}^{n} \left(\lambda_m \frac{d}{dt} \delta x_m + \dot{\lambda}_m \delta x_m \right) \tag{C10}$$

Using (C9) and (C7) we have:

$$\frac{d}{dt} \left(\sum_{m=1}^{n} \lambda_m \delta x_m \right) = \sum_{m=1}^{n} \left[\lambda_m \left(\sum_{i=1}^{n} \frac{\partial f_m}{\partial x_i} \delta x_i \right) - \left(\sum_{i=1}^{n} \frac{\partial f_i}{\partial x_m} \lambda_i \right) \delta x_m \right]$$

$$= 0$$

Thus:

$$\sum_{m=1}^{n} \lambda_m \delta x_m = \text{constant} \tag{C11}$$

And:

$$\sum_{m=1}^{n} \lambda_m^f \delta x_m^f = \sum_{m=1}^{n} \lambda_m^o \delta x_m^o \qquad \text{(C12)}$$

But by (C4)

$$x_j^f = g_j(x_1^o, x_2^o, \ldots x_n^o) \qquad j = 1, 2, \ldots n$$

$$\delta x_j^f = \sum_{i=1}^{n} \frac{\partial g_j}{\partial x_i^o} \delta x_i^o \qquad \text{(C13)}$$

Combining (C12) and (C13) we have:

$$\sum_{m=1}^{n} \left[\lambda_m^f \left(\sum_{i=1}^{n} \frac{\partial g_m}{\partial x_i^o} \delta x_i^o \right) \right] = \sum_{m=1}^{n} \lambda_m^o \delta x_m^o$$

And:

$$\sum_{m=1}^{n} \left(\sum_{i=1}^{n} \lambda_i^f \frac{\partial g_i}{\partial x_m^o} \right) \delta x_m^o = \sum_{m=1}^{n} \lambda_m^o \delta x_m^o$$

But δx_m^o are all independent, so :

$$\lambda_m^o = \sum_{i=1}^{n} \lambda_i^f \frac{\partial g_i}{\partial x_m^o} \qquad m = 1, 2, \ldots n \qquad \text{(C14)}$$

QED

NASA-Langley, 1966 CR-394